Accepted Manuscript

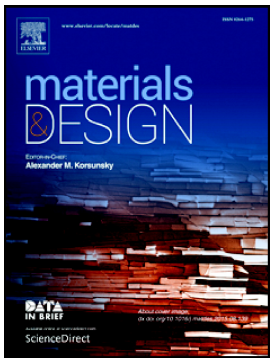

Anisotropy in the quasi-static and cyclic behavior of ZK60 extrusion: Characterization and fatigue modeling

A.H. Pahlevanpour, S.M.H. Karparvarfard, S.K. Shaha, S.B. Behravesh, S. Adibnazari, H. Jahed

PII: S0264-1275(18)30780-9
DOI: doi:10.1016/j.matdes.2018.10.026
Reference: JMADE 7440

To appear in: *Materials & Design*

Received date: 27 June 2018
Revised date: 21 September 2018
Accepted date: 15 October 2018

Please cite this article as: A.H. Pahlevanpour, S.M.H. Karparvarfard, S.K. Shaha, S.B. Behravesh, S. Adibnazari, H. Jahed , Anisotropy in the quasi-static and cyclic behavior of ZK60 extrusion: Characterization and fatigue modeling. Jmade (2018), doi:10.1016/j.matdes.2018.10.026

Anisotropy in the Quasi-static and Cyclic Behavior of ZK60 Extrusion: Characterization and Fatigue Modeling

AH. Pahlevanpour[1-2], SMH. Karparvarfard[1], S.K. Shaha[1], S.B. Behravesh[1], S. Adibnazari[2], H. Jahed[1*]

[1]Deparment of Mechanical & Mechatronics Engineering, University of Waterloo, 200 University Ave W, Waterloo, ON N2L 3G1, Canada

[2]Department of Aerospace Engineering, Sharif University of Technology, Azadi Street, Tehran, Iran

Abstract

The quasi-static and strain-controlled fatigue characteristics of ZK60 extrusion have been investigated along three different directions: the extrusion direction (ED), the radial direction (RD), and 45° to the extrusion direction (45°). The quasi-static response showed symmetric behavior for the samples tested along RD and 45°, whereas the ED samples manifested completely asymmetric behavior. Although the ED samples exhibited longer fatigue lives than the RD and 45° in the high cycle fatigue, the fatigue lives in the low cycle fatigue regime were similar. The texture measurement indicated a sharp basal texture along ED, explaining its asymmetric behavior. Higher tensile mean stress and less dissipated plastic energy per cycle for the ED samples, acting as two competing factors, were the principal reasons for exhibiting fatigue responses identical to those of RD and 45° in the LCF regime. The fracture surface in the ED direction was dominated by twin lamellae and profuse twinned grains, whereas that in RD was dominated by slip bands. Finally, Smith-Watson-Topper and Jahed-Varvani models were employed to predict the fatigue lives along all directions using a single set of material parameters.

Keywords: ZK60 extrusion, Anisotropy, Asymmetry, Texture, Characterization, Fatigue Modeling

1. Introduction

Light-weighting is one of the pivotal steps toward fuel consumption reduction in vehicles and consequent environmental preservation. Magnesium (Mg) alloys, as the lightest engineering metal, could contribute to this process. However, they should be well characterized in order to elucidate their properties for the automotive industry [1]. In spite of the wide implementation of Mg alloys in many non-structural automotive components, their current application in load-bearing sections is limited [2]. To expand their application in load-bearing components, it is of key importance to investigate Mg alloys' behavior under both static and cyclic loading.

The hexagonal close-packed (HCP) crystal structure of Mg brings about a strong basal texture in its wrought alloys [3]. As they undergo forming processes, such as rolling and extrusion, the basal planes will be lined up parallel to the working direction. This intense crystallographic texture will make the $\{10\bar{1}2\}$ pyramidal twin the dominant deformation mechanism under certain loading

* Corresponding author, hamid.jahed@uwaterloo.ca

directions where tension along the c-axis is triggered [4]–[6]. Reversing the load will reorient the twinned crystals toward their initial state; this process is known as detwinning. Twinning-detwinning engenders highly distorted asymmetrical hysteresis loops, mainly in the twinning-induced regions [7], [8]. The directional dependency of twinning-detwinning renders not only the quasi-static tension and compression behaviors but also the fatigue properties of wrought Mg alloys, and so has been widely investigated for such alloys [9]–[12].

Anisotropy in Mg alloys can affect the fatigue strength differently in the high-cycle fatigue (HCF) and low-cycle fatigue (LCF) regimes. Sajuri et al. [13] reported that the HCF strength of AZ61 extrusion along the extrusion direction (ED) in stress-controlled experiments is higher than that in the transverse direction (TD) and 45° to the ED. The same characteristic was observed under controlled strain by Jordon et al. [14] for AM30 extrusion in the HCF regime, even though for LCF, loading along ED yields lower life to failure than along TD. Roostaei and Jahed [15] investigated the effect of loading direction on the LCF fatigue characteristics of AM30 extrusion. They reported that TD specimens failed in higher lives when identical strain amplitude is applied to both TD and ED specimens. In contrast, Wang et al. [16] found the opposite while testing ED against TD samples under the strain-control state for ZA81M extrusion, a result they attributed to strengthened twinning deformation as well as to the higher detrimental tensile mean stresses in TD. Xiong and Jiang [17], while experimentally scrutinizing the LCF behavior of AZ80 rolled in four different orientations found that deformation mechanism alteration at a certain strain level affects the material's fatigue resistance with respect to the loading direction. The AZ80 samples in the rolling direction (RD) have the longest life of all other directions for strain amplitudes of less than 0.4%, but increasing the strain to higher values causes the 30° and 60° inclined samples with respect to the rolled plane to exhibit higher fatigue strength.

ZK60, the material under study in this paper, exhibits exceptional strength and ductility due to its alloying elements [18]. However, despite these characteristics, only limited studies have investigated its fatigue characteristics in extrusion form. Xiong et al. [19], [20] and Yu et al. [21] have studied LCF and cyclic plastic deformation, and Wu et al. [22] explored twinning–detwinning behavior of ZK60 extrusion along the ED. These studies reported asymmetry in both the quasi-static behavior and the cyclic hysteresis loops. In more recent study by Xiong et al. [23], characterizing ZK60 under monotonic loading along ED and TD revealed intensive anisotropy in the stress-strain response of the material. The reviewed literature discloses a lack of knowledge on the HCF behavior of ZK60 along directions other than ED.

Numerous fatigue damage criteria have been developed and reviewed over the last two decades [24]–[33]. However, most of these criteria have been developed and calibrated for isotropic materials, with dislocation slip being the dominant deformation mechanism. Due to slip dislocation, intergranular and transgranular cracking along the slip lines are the primary cracking behavior under cyclic loading for isotropic material [34]. However, the twinning-detwinning deformation mechanism adds micro-cracking on the twin boundaries as a third mode in Mg alloys [34]. This additional deformation mechanism and its detrimental effects should be reflected in the fatigue damage models proposed for Mg and its alloys. The scalar inherence of energy allows the simple manipulation of the energy values corresponding to the axial and shear components of stress/strain tensors. This feature suggests that strain energy is a good candidate for fatigue damage representation in anisotropic materials. Jahed and Varvani proposed a fatigue model based on the strain energy dissipated in each cycle of loading and on the dominant cracking mechanisms [35].

This model has been widely employed in many related types of research on Mg alloys [15], [36] exhibiting promising results. They improved the capability of the original model to make it applicable to non-proportional loading by adopting Garud's incremental cyclic plasticity model [37], [38]. This extended model has shown promising life estimation for AZ31B under proportional and non-proportional loading in research by Albinmousa and Jahed [39]. Roostaei and Jahed showed that the Smith-Watson-Topper (SWT) and Jahed-Varvani JV parameters yield acceptable life prediction for AM30 extrusion along the different loading directions [15].

Smith–Watson–Topper (SWT) was introduced as a critical plane approach for modeling material in which fatigue cracks are initiated and grew predominantly under tensile loading [40]. Tensile cracking developed in ZK60 extrusion along ED was implied by a single curve description of the SWT parameter in less than 1.5% strain amplitudes [21]. A similar justification was provided to explain imprecise SWT life estimation when the strain amplitude was increased to larger than or equal to 3.5%, the amplitudes where ED samples fail under compressive loading [19].

This present investigation, therefore, begins with the microscopic characterization of ZK60 extrusion. The cyclic behavior of the material, including its strain-life and stabilized strain-stress response together with fractographic observations, will be presented and rigorously discussed with reference to three different directions: namely, ED, RD, and 45° to ED (45°). Finally, the merits of SWT as a critical plane and JV as an energy-based model will be assessed based on their capability of mimicking experimental data.

2. Material and Experimental Details

2.1. Material and Specimen

The material investigated in this study, ZK60A Mg alloy in the form of an extruded cylindrical billet with a 127mm diameter, has the chemical composition of Zn 5.5%, Zr 0.71%, other 0.3%, and the balanced weight percent of Mg. The static and fatigue specimens geometry is depicted in Figure 1 (a) and (b). In order to investigate the anisotropy effect of loading directions, specimens were extracted along three distinctive directions, labeled ED, RD, and 45°, such that gage sections were located at the same radius for all samples. The reference cylindrical coordinate system for specimen extraction relative to the extruded billet is illustrated in Figure 1 (c). ED, RD, and TD denote the extrusion, radial, and tangential directions, respectively.

2.2. Experimental Procedures

For microstructural observation, samples were prepared through the following standard metallographic procedure. First, they were ground using silicon carbide papers with grit No. up to 1200 and polished sequentially with 6, 3, 1 and 0.1 micron diamond pastes. In order to reveal the grain/twin boundaries, etchant made of 4.2 g picric acid, 70 ml ethanol, 10 ml acetic acid, and 10 ml distilled water was applied to the sample surface.

Figure 1. (a) Static tension and fatigue test specimens geometry, (b) Static compression test specimen geometry, and (c) Reference cylindrical coordinate system for sample extraction (Dimensions are in "mm")

The crystallographic texture was characterized by means of X-ray diffraction employing Bruker D8 Discover X-ray diffractometer equipped with an advanced 2D-detector. The characterization started with measuring incomplete pole figures in the back-reflection mode applying CuKα radiation at 40 kV-40 mA. The complete pole figures were generated using DIFFRAC.texture software. The details of the texture measurement are elaborated in [41].

Quasi-static tests were conducted on Instron 8872 servo-hydraulic axial test frame with 25kN load capacity at the ambient temperature. Dog-bone and cuboid samples were used for the static tension and static compression tests, respectively. In these tests, displacement was controlled in order to maintain the strain rate at 0.015 mm/mm/min in accordance with ASTM E8 [42], while the strain was measured using digital image correlation (DIC) technique.

Fully reversed strain-controlled fatigue tests were performed on the same Instron test frame. These tests were conducted at different strain amplitudes, (R=-1) ranging from 0.2 to 2 %, with at least two trials at each amplitude. The test frequency was selected based on the applied strain amplitude, varying from 0.1 Hz to 10 Hz, to guarantee precise control of the sinusoidal waveform of the strain. The strain was measured by Instron extensometer with a 10 mm gauge length and ±1 mm travel. The fatigue failure was set at 50% drop in the peak tensile force of the stabilized cycle or the final fracture and the test is considered run-out if the sample survives for more than 1 million cycles. Selected fracture samples were analyzed using scanning electron microscope (SEM) to understand the fracture mechanisms.

3. Results

3.1. Microstructure Analysis

The microstructural examination of ZK60 extrusion, shown in Figure 2, disclosed the twin-free bimodal grains, i.e., sizable elongated and small equiaxed grains. Similar microstructural characteristics have been reported for this material [21], [43].

Figure 2. Typical microstructure of ZK60 extrusion: (a) TD-RD plane and (b) RD-ED plane

The pole figures, plotted for both RD-TD and ED-RD planes in Figure 3, revealed that the majority of the c-axes are oriented approximately perpendicular to the ED, but not necessarily parallel to the RD or TD. The crystallographic orientation matches those observed in earlier studies on ZK60 extrusion [23], [43]. This can favor $\{10\bar{1}2\}$ extension-twinning under compression loading in ED samples [22], [23]. The effect of this texture on quasi-static and cyclic behaviors will be thoroughly discussed later.

Figure 3. (0002) and $(10\bar{1}0)$ pole figures of ZK60 extrusion obtained from: (a) TD-RD plane and (b) ED-RD plane

3.2. Quasi-static Tension and Compression Behavior

Figure 4 illustrates the engineering stress-strain curves for ZK60 extrusion under quasi-static tensile and compressive loadings along different directions. It is seen that the tensile and compressive yield strengths along ED are 251 MPa and 128 MPa, respectively. In contrast, similar

yield strengths are observed along the other two directions, i.e., the average yield strengths of 130 MPa and 136 MPa, along RD and 45°, respectively. Table 1 summarizes the quasi-static mechanical properties of the material along these directions. Two tests were averaged to get the value for each property. The ductility along ED is less than that along RD and 45°, which is in agreement with the texture results, indicating that the c-axes of the grains are perpendicular to the ED. Hence, less number of slip modes can be activated to accommodate the strain.

Figure 4. Quasi-static behavior under tensile and compressive loading for ED, RD, and 45°

Table 1. Quasi-static mechanical properties of ZK60 extrusion along different directions (The numbers in the parentheses are standard deviations)

Mechanical properties	ED	RD	45°
Module of elasticity [GPa]	43 (1)	45 (0)	42 (1)
Tensile yield strength [MPa]	251 (0)	128 (0)	149 (2)
Tensile ultimate strength [MPa]	309 (1)	279 (1)	264 (1)
Ductility (%)	11 (0)	23 (1)	26 (0)
Compressive yield strength [MPa]	128 (10)	132 (4)	123 (5)
Compressive ultimate strength [MPa]	449 (15)	357 (9)	388 (3)

3.3. Cyclic Behavior

3.3.1. Extrusion Direction

Figure 5 depicts the typical engineering stress-strain hysteresis loops of the stabilized cycles for total strain amplitudes between 0.2% and 2% for the ZK60 extrusion along ED. It is observed that the hysteresis loops for the strain amplitudes lower than 0.5% are not sigmoidal. In contrast, increasing the strain amplitudes to more than 0.5% brings about a sigmoidal-shape hysteresis loop. Such asymmetry indicates the activation of twinning and detwinning upon compressive and tensile reversals, respectively [44].

Figure 5. Typical engineering stress-strain hysteresis loops of the stabilized cycle for ED ranging from 0.2% to 2% strain amplitudes

To be more specific, the evolutionary change of hysteresis loops from the second cycle to the stabilized cycle is depicted in Figure 6. One of four distinct behaviors is applicable depending on the applied strain amplitude: (i) symmetric without twinning ,(ii) partially asymmetric ,(iii) asymmetric, and (iv) "leading-to-symmetric" behavior. First, at low strain amplitudes (lower than 0.4%), the stabilized hysteresis loops are symmetric, implying that the stress is insufficient to activate extension-twinning under compression loading [45]. At such low strain amplitudes, the deformation mechanism is controlled by the gliding of dislocations [22]. Moreover, marginal cyclic hardening is observed in Figure 6 (a), probably due to the increased density of dislocations with the increasing number of cycles [46]. For the strain amplitudes of 0.5%, Figure 6 (b), the hysteresis loop at the second cycle is asymmetric in tension and compression reversals, denoting

that twin and detwin deformations are active. Activation of the extension twin in a compression reversal results in an 86.3° rotation in crystal orientation [47]. Therefore, the twinned grains are likely to detwin during the subsequent tension reversal [22]. Nevertheless, the twinned grains in the compression reversal are not fully detwinned in the following tension reversal, leading to the formation of residual twins and cyclic hardening [39]. However, the hysteresis loop at the stabilized cycle exhibits no sign of twinning dominance, and therefore the slip of dislocations is accommodating the applied strain. It is believed that this change in the deformation behavior is due to the exhaustion of the new extension twin. This behavior has already been observed in ZK60 [21] and AM30 [15] along ED.

Figure 6. Evolution of hysteresis loops for 2nd and stabilized cycles along ED at different strain amplitudes: (a) 0.3%, (b) 0.5%, (c) 0.8%, and (d) 2%

As the applied strain amplitude is increased (to more than 0.5%), Figure 6 (c), the stresses during compressive reversals are high enough to activate the extension-twinning. The twinned grains formed under compression are partially detwinned in the next tensile reversal, resulting in residual twins. These residual twins build up resistance to the plastic deformation in the wake of their interactions with dislocations and twinned grains which brings about cyclic hardening [22][48]. Lastly, when the strain amplitude reaches to as large as 2%, Figure 6 (d), twinning governs the plastic deformation in the compressive reversal of the first few cycles. During the tensile reversal, detwinning occurs inside the twinned grains, and after detwinning exhausts, non-basal slips accommodate strain [17]. As a result, the hysteresis loop for the second cycle is sigmoidal for the tensile reversal. However, as the number of cycles increases, the compressive reversal also tends to the sigmoidal shape, as twinning is exhausted before the end of compressive reversal. The subsequent concave-down curve is as a result of the competitive twinning and slip mechanisms [20]. In contrast, the tensile reversal demonstrates cyclic softening, which is due to the incessant formation of micro-cracks in the first few cycles with limited growth at such a high strain amplitude. These micro-cracks alleviate deformation under tension which would be generally hindered by residual twin. As a result, less tension is required to achieve the intended strain level leading to the softening behavior. In contrast, the micro-cracks are closed under compression and consequently cannot accommodate the deformation [49]. It is also reported that the annihilation and rearrangement of dislocations can cause this softening [22]. As a result of cyclic hardening in the compressive reversals and cyclic softening in the tensile reversals, hysteresis loops tend to be tension-compression symmetric. Similar behavior has been observed in AM30 extrusion for strain amplitudes greater than 1.5% [15].

3.3.2. Radial Direction

Typical engineering stress-strain hysteresis loops along RD for ZK60 extrusion are plotted in Figure 7 at different strain amplitudes ranging from 0.2% to 2%. At all strain amplitudes, the hysteresis loops are roughly symmetric, unlike those in the ED. Slip is the dominant deformation mechanism at small strain amplitudes; however, twinning is also happening at high strain amplitudes ($\varepsilon_a \geq 1.6\%$) and forms sigmoidal-shape hysteresis loops. It is also observed that the peak stresses in the compression reversals are larger than those in the tension ones. As indicated in Figure 8, there is no such a difference between the second hysteresis and the stabilized one along RD. This is because of the lack of residual twins in this direction, the reason of which will be

discussed later. Thus, larger compressive peak stresses comparing to the tensile ones stem from the quasi-static behavior. Returning to section 3.1 and Table 1, it was stated that along RD, the compression yield strength is greater than the tension yield; thereby, higher peak stress is eventually achieved under compression reversal.

Figure 7. Typical engineering stress-strain hysteresis loops of the stabilized cycle for RD ranging from 0.2% to 2% strain amplitudes

According to Figure 8, at the strain amplitude of 1%, the second and stabilized hysteresis loops do not show a remarkable decrease of hardening rate under compressive reversal, indicating that twinning is not happening massively. In fact, the crystal orientations in some grains favor the activation of extension-twinning under both reversals, and consequently, detwinning partially reorients the twinned grains under both tension and compression loading. As a result, few residual twins remain in the microstructure; hence, slight strain hardening occurs both in tension and compression reversals due to the twin-twin and twin-dislocation interactions. On the other hand, as the strain amplitude is increased to 2%, the non-basal slip modes are activated in addition to the twinning and detwinning, which results in the sigmoidal hysteresis loop. However, for the reason mentioned before, only a limited number of residual twins remain in the microstructure. Marginal cyclic hardening can be observed by comparing the stabilized and second cycle hysteresis loops.

Figure 8. Evolution of hysteresis loops for 2nd and stabilized cycles along RD at the strain amplitude of (a) 1% and (b) 2%

3.3.3. 45° Direction

Figure 9 shows the typical engineering stress-strain hysteresis loops along 45° for ZK60 extrusion at strain amplitudes ranging from 0.3% to 2%. The stabilized fatigue response, like the one along RD, does not show a low-hardening section under compressive and tensile reversals up to the strain amplitude of 1%. However, the sigmoidal behavior along 45° differs from that along RD, i.e., the peak stresses and strain hardening are slightly higher in tension reversals. This, again like RD, is stemming from the quasi-static behavior of 45°.

Hysteresis loop evolution along 45° is shown in Figure 10. As seen in Figure 10 (a), the hysteresis loop evolution along 45° at the strain amplitude of 1% is similar to that along RD; i.e., very marginal cyclic hardening is observed under both tension and compression loading. However, at the strain amplitude of 2%, Figure 10 (b), the behavior is more similar to that in the ED direction; i.e., after the first few cycles, cyclic softening on the tensile side and cyclic hardening on the compressive side can be seen. However, in the case of 45°, softening is not as severe as that along ED.

Figure 9. Typical engineering stress-strain hysteresis loops of the stabilized cycle for 45° direction ranging from 0.3% to 2% strain amplitudes

Figure 10. Evolution of hysteresis loops for 2nd and stabilized cycles along 45° direction at the strain amplitudes of (a) 1% and (b) 2%

3.4. Strain-life Curve

The strain-life (ε_a-N) curves for ZK60 extrusion along different directions are depicted in Figure 11. It is noteworthy that both the 45° and RD samples are displaying the same life at different strain amplitudes. Moreover, comparing the fatigue responses along RD and ED, it is noted that the lives are similar for the strain amplitudes of 0.4% and higher (the low cycle fatigue regime). However, in the high cycle fatigue regime (strain amplitudes of 0.3% and lower), the cyclic respond depends on the material direction. For instance, while the fatigue life at the strain amplitude of 0.3% along RD is ~ 27000 cycles, that for ED is improved to ~ 100,000 cycles. While the run-out test for ED happened at the strain amplitude of 0.25%, RD samples exhibited an average life of 90,000 cycles at the same strain amplitude. The run-out test for RD was achieved at 0.2%. The reasons for the similar fatigue performance in the low cycle fatigue (LCF) for all directions, but not in the high cycle fatigue (HCF) will be discussed later.

Figure 11. A comparison of strain-life (ε_a-N) curves obtained from different directions for the ZK60 extrusion

3.5. Fatigue Fracture Surfaces

The SEM images of the fatigue fracture surface of ED, RD, and 45° samples at two strain amplitudes of 0.3% and 2% are presented in Figure 12. Multiple crack initiation sites (marked by yellow arrows) are visible for all directions at the higher strain amplitude, whereas crack initiation sites are fewer at the lower strain amplitude. The fatigue failure (FF) area is distinguished from the fatigue crack growth (FCG) zone by dashed lines, and generally, at lower strain amplitudes, the FCG area is larger, manifesting a longer fatigue life. Yellow arrows indicate the position of crack initiation sites.

Figure 12. SEM images of fatigue fracture surfaces of ZK60 extrusion Mg alloy at different strain amplitudes along different directions: (a) ED at ε_a =0.3%, (b) ED at ε_a =2%, (c) RD at ε_a =0.3%, (d) RD at ε_a =2%, (e) 45° at ε_a =0.3%, and (f) 45° at ε_a =2%

The fracture surfaces at higher magnifications are shown for the strain amplitude of 2% along different directions in Figure 13. Twin lamellae are observed on the fracture surface of ED samples, whereas RD fracture surface reveals slip bands (SB).

Figure 13. SEM images of the fracture surface of ZK60 extrusion at the total strain amplitude of 2% showing twin lamellae and slip bands on the (a) ED sample and (b) RD sample

Figure 14 illustrates the FCG zone of ZK60 at the total strain amplitudes of 0.3% and 2%. Fatigue striations (FS) marks are denoted on the images. Each striation mark represents the propagation of the fatigue crack in one cycle. Hence, the finer the marks, the longer the fatigue life. While the average distance between the FS marks for the ED sample under strain amplitude of 0.3% was 0.6±0.16 μm, the RD and 45° samples exhibited striations with an average distance of 1.92±0.3 μm, which is a testimony to the longer fatigue life along ED. In contrast, the average distance along FS marks along ED, RD, and 45° directions under strain amplitude of 2% were 2.14±0.04 μm, 2.01±0.09 μm, and 2.21±0.43 μm, asserting the similar lives in the LCF regime.

Figure 14. Fatigue crack growth at the total strain amplitudes of 0.3% (Top) and 2% (Bottom) for (a) ED, (b) RD, and (c) 45° samples

Lastly, to be more specific, the microstructure of the fatigue fractured samples tested at the strain amplitude of 2% along (a) ED and (b) RD are shown in Figure 15. Profuse twinned grains are observed in the microstructure along ED; however, the twinned area in the RD sample was significantly lower. This is in agreement with the hysteresis loops obtained in section 3.3, in that the ones for ED samples were less symmetric, as twinning was more dominant.

Figure 15. Microstructure illustrating the traces of twin on the polished cross-section of the fatigue-tested samples near the fracture surface, obtained at a strain amplitude of 2% along (a) ED and (b) RD

4. Discussion

4.1. Deformation Behavior

The development of hysteresis responses along different directions during the fatigue tests was discussed in the previous sections. The mechanical behavior of the material is highly associated with the crystallographic texture, which controls the active modes of deformation. It is well-established that $\{10\bar{1}2\}$ extension-twin can accommodate plastic strain in HCP crystal structures when the applied loading is either tensile along the c-axes of the grains, or compressive perpendicular to the c-axes [22]. This polar nature of twinning brings about evident tension-compression asymmetric behavior in wrought Mg alloys [50]. For ZK60 extrusion, along ED, extension-twinning drives the deformation only under compressive loading. However, for the radial and 45° directions, twinning can happen under both tensile and compressive reversals. Consequently, in each reversal, some of the grains' orientation favors the activation of twinning, while the other pre-twinned grains tend to detwin. Therefore, hysteresis loops along these directions are less asymmetric compared to ED.

Figure 16 depicts the cyclic tension and compression behaviors of ZK60 along the three directions. The plots are constructed from the peak stresses of the stabilized hysteresis loops. It is noted that both the cyclic tension and cyclic compression curves for 45° are located between the curves of ED and RD. This observation suggests that the deformation mechanism, as a

macroscopic consequence of texture, along the 45° direction is a combination of the activated mechanisms along ED and RD.

Figure 16. Cyclic tension and compression behaviors along ED, RD, and 45°

In Figure 17, the term Asymmetric Ratio (AR) = $\frac{TS-CS}{TS+CS}$ refers to the level of asymmetry, where TS and CS are the tensile peak stress and compressive peak stress, respectively. For a symmetric cyclic behavior, the asymmetry level equals zero, whereas the positive and negative levels of asymmetry reveal higher tensile peak stress and higher compressive peak stress, respectively. Asymmetry is clearly evident along ED up to the strain amplitude of 1%, but then decreases drastically, probably due to the formation of micro-cracks, and consequently reduces the tensile peak stress. The annihilation and rearrangement of dislocations, which together can decrease the post-detwinning dislocation-based flow, can also cause this softening, as reported in the literature [20][22][49][41].

Figure 17. Ratio of cyclic asymmetry at different strain amplitudes ranging from 0.3 to 2% for different sample orientations

The RD asymmetry levels do not change remarkably, remaining close to zero, and so manifesting more symmetric behavior than other directions. As discussed, this symmetric behavior arises from the crystallographic texture of ZK60 extrusion, in which the c-axes of grains are randomly orientated on a plane normal to ED. Hence, twinning happens under both tension and compression along RD. Lastly, along 45°, like the deformation curves, the level of asymmetry lies between the ones for ED and RD, signifying that the deformation behavior of 45° is a combination of ED and RD behaviors. Moreover, while the asymmetry level for 45° is not as high as ED's owing to different texture, it decreases like ED's at high strain amplitudes. A finding that can be attributed to the tension peak stress drop at high strain amplitudes (Figure 10).

In Figure 18, the tension and compression cyclic behavior of ZK60 is plotted against the quasi-static behavior under tension and compression loadings along different material directions. At low strain amplitudes, where the material response is nearly elastic, the quasi-static and cyclic behaviors are very similar. However, at higher strain amplitudes, cyclic hardening occurs due to the resistance built up by dislocation-dislocation, dislocation-twin, and twin-twin interactions [20]. Hence, cyclic curves are harder than quasi-static curves for RD and 45°. However, as previously stated, for ED, softening occurs at strain amplitudes higher than 1%, probably due to the formation of micro-cracks, and affects fatigue modeling, as discussed later.

Figure 18. Comparison between quasi-static and cyclic curves for ZK60 extrusion along (a) ED, (b) RD, and (c) 45°

4.2. Effect of Loading on the Fatigue Performance

Figure 11 showed that the fatigue life of ZK60 is not sensitive to the material direction in the

LCF regime, i.e., $\varepsilon_a \geq 0.4\%$, although the deformation behavior differs. In other words, the cyclic deformations for RD and 45° are almost symmetric, whereas the deformation for ED involves profound twinning happening only under compressive loading. Thus, significant asymmetry is evident. On the other hand, according to Figure 11, fatigue life within the HCF regime, i.e., $\varepsilon_a < 0.4\%$, is distinct in spite of similar symmetric deformation behavior.

Figure 19 demonstrates the hysteresis loops at two different strain amplitudes, 0.5% and 1%, both corresponding to the LCF regime, for different directions. Although the tensile peak stresses for ED are the highest among all directions for both strain amplitudes, the areas inside the ED hysteresis loop are less than those of RD and 45°. The area inside a hysteresis loop represents the energy being dissipated in each cycle. Therefore, less energy would dissipate along ED in each cycle than along the other two directions, both of which show relatively similar loop areas. On the other hand, the larger tensile peak stress causes wider stress ranges and higher tensile mean stresses, which are more damaging for ED samples.

Figure 19. Stabilized hysteresis loops for ED, RD, and 45° at (a) ε_a =0.5% and (b) ε_a =1%

Profound residual twins can affect the fatigue life of ED samples in two ways. Firstly, interactions between twin-twin bands and twin-dislocations can initiate cracks, leading to premature fatigue failure [41][51]. On the other hand, some studies have suggested that the surface roughness as a result of extension-twinning can retard crack growth, due to roughness-induced crack closure [52]. The overall result of competing factors, namely strength, twin-twin bands interactions, twin-dislocations interactions, and surface roughness resulting from extension-twinning, is that the fatigue lives in the LCF regime are similar. However, in the HCF regime where twinning does not happen, material's strength governs deformation. In fact, at these strain amplitudes, the area inside the hysteresis loop is small, indicating little plasticity in the deformation. The deformation thus tends to be more elastic, and so the governing fatigue life factor in the HCF regime would be the strength of the alloy, suggesting a remarkably higher fatigue life for ED samples in HCF because cracks initiation occurs later due to the higher strength along this direction [53].

5. Fatigue Modeling

As discussed, ZK60 extrusion exhibits identical behavior in the LCF regime along three different directions in terms of the strain-life curve; however, in the HCF regime, their fatigue response shows segmental deviation. Furthermore, along the ED, there is a partial softening in the high strain amplitude, e.g., ε_a =1.6% compared to 1 %, which causes nonlinearity in the elastic strain response of the material, when plotted with respect to the number of reversals (Figure 20 (a)). As a consequence, the fatigue modeling of ZK60 can be complex. A goal in fatigue modeling of anisotropic materials is to discover a set of universal parameters that can be employed for life prediction of the material regardless of the orientation. To this intent, RD was selected as the primary direction, and the universal parameters required for two different damage criteria were extracted from the experiments in this specific direction. Eventually, these parameters were used to predict the life in other directions. In what follows, SWT, as a critical plane model, and JV, as an energy-based damage criterion, are assessed for the fatigue life prediction of ZK60.

5.1. SWT

The SWT parameter was founded on the principal strain range and maximum stress on the principal strain plane, namely $\Delta\varepsilon_1$ and $\sigma_{n,max}$, respectively, in the following formulation:

$$SWT = \sigma_{n,max}\frac{\Delta\varepsilon_1}{2} \quad \textbf{Eq. 1}$$

This parameter was originally suggested to account for the mean stress effect and has been extensively employed in many efforts to estimate the fatigue life of Mg alloys [15], [19], [21], [41], [54], [55]. Although the SWT parameter was defined the same in all those studies, its correlation with fatigue life was made differently. In the present study, the correlation is formulated by integrating SWT with the Coffin-Manson relation as follows:

$$SWT = \frac{{\sigma'_f}^2}{E}\left(2N_f\right)^{2b} + \sigma'_f\varepsilon'_f\left(2N_f\right)^{b+c} \quad \textbf{Eq. 2}$$

where:

σ'_f: Fatigue strength coefficient

ε'_f: Fatigue toughness coefficient

b: Fatigue strength exponent

c: Fatigue toughness exponent

and E is the modulus of elasticity and $2N_f$ is the number of reversals to failure. Other components on the right side of the equation are based on the Coffin-Manson approximation and will be extracted by employing strain-life and hysteresis curves along RD. In this approach, the strain range is decomposed into elastic and plastic parts ($\Delta\varepsilon_e$ and $\Delta\varepsilon_p$), which are calculated from the stabilized hysteresis loop for each strain amplitude:

$$\frac{\Delta\varepsilon_e}{2} = \frac{\sigma'_f}{E}\left(2N_f\right)^b \quad \textbf{Eq. 3}$$

$$\frac{\Delta\varepsilon_p}{2} = \varepsilon'_f\left(2N_f\right)^c \quad \textbf{Eq. 4}$$

The elastic and plastic strain ranges with respect to the number of reversals to failure are depicted in Figure 20 (b). The Coffin-Manson parameters, as presented in Table 2, were extracted from the experimental results in the reference direction (RD) using the aforementioned equations.

Table 2. Coffin-Manson parameters for SWT model

σ'_f (MPa)	360.73
ε'_f	1.862

b	-0.110
c	-0.780

Finally, by substituting these parameters into the SWT model (Eq. 1 and 2), the predicted lives in all three directions were found through a numerical solution.

Figure 20. (a) Nonlinear elastic response of the strain for ED and (b) decomposition of strain into elastic and plastic strain in RD

The predicted lives in contrast to the experimental ones are illustrated in Figure 21. A diagonal solid line denotes the ideal prediction, while the dashed and dashed-dot lines specify the area where predicted life over experimental life rests within the factors of 2 and 2.5, respectively. Along RD, life prediction meets expectation in accordance with the fact that the Coffin-Manson parameters were extracted in this direction. For both 45° and ED specimens, SWT underpredicts the life; however, the prediction is more conservative for ED. The observed drop in the life prediction accuracy of ED might be attributed to the reported nonlinear elastic strain of the material, which is fitted by the linear regression in the Coffin-Manson relation (Figure 20 (a)).

Figure 21. SWT predicted vs. experimental reversals for all directions

5.2. Jahed-Varvani

As was pointed out and discussed earlier, the anisotropic properties of wrought Mg alloys could make their fatigue modeling challenging. Due to the scalar nature and resulting direction independency of energy, the longstanding approach to tackling this exceptional characteristic is implementing energy-based damage parameters, including JV, Jiang, and Ellyin [9], [15], [39], [41], [54]–[58]. In JV, total strain energy, as the damage parameter, is expressed by two terms: i) the positive elastic strain energy density (ΔE_e^+), and ii) the plastic energy density (ΔE_p). The latter is defined as the area inside the hysteresis loop, and the former is obtained by the following equation:

$$\Delta E_e^+ = \frac{{\sigma_{max}}^2}{2E} \qquad \textbf{Eq. 5}$$

where σ_{max} is the tensile peak stress. By assembling the elastic and plastic parts of strain energy, the JV parameter is formulated thus:

$$JV = \Delta E_e^+ + \Delta E_p \qquad \textbf{Eq. 6}$$

and will be correlated to life as follows [35]:

$$JV = E_e'\left(2N_f\right)^B + E_f'\left(2N_f\right)^C \qquad \textbf{Eq. 7}$$

where the four parameters on the right side of the equation are

E'_e = Energy-based fatigue strength coefficient
E'_f = Energy-based fatigue ductility coefficient
B = Energy-based fatigue strength exponent
C = Energy-based fatigue ductility exponent

These parameters are determined from curves fitted to the elastic and plastic portions of the energy along the radial direction, as depicted in Figure 22 (a).

Table 3. JV model parameters

E'_e (MJ/m^3)	1.4875
E'_f (MJ/m^3)	1604.3
B	-0.219
C	-0.920

Figure 22. (a) Decomposition of total strain energy into elastic and plastic energies in RD and (b) JV predicted vs. experimental reversals for all directions

By employing the JV model in conjunction with the parameters extracted for RD, Table 3, fatigue lives in different directions are predicted numerically similar to the SWT approach and plotted against the experimental life in Figure 22 (b). The data-points congregating about the solid line and almost within the bound of factor 2.5 in both LCF and HCF regions demonstrate the capability of the JV parameter to model the fatigue of ZK60 with anisotropic behavior. However, some deviation is observed along the ED direction as the lives increases to more than 10000 cycles. This deviation is possibly attributed to exhausted plastic energy decapitation through the hysteresis loops in HCF where the model relies solely on the elastic part of the strain energy. Comparing the Figure 21 and Figure 22 (b) suggests that the SWT model yields to more conservative life predictions than the JV model.

5.3. Further Discussion

The total strain energy density, as a fatigue damage parameter, is determined at each strain amplitude at the stabilized cycle to discern the underlying reason for similar LCF lives, but different HCF ones. Figure 23 depicts the total strain energy density against the total strain amplitude for the different directions. It is observed that at high strain amplitudes, although the deformation behaviors are dissimilar, the fatigue damage parameters are roughly the same. Therefore, the fatigue lives in the LCF regime are identical in the wake of similar fatigue damage occurring. On the other hand, under small strain amplitudes, i.e., the HCF regime, the amount of damage at the stabilized cycle is marginal and close to zero, implying elastic deformation.

Figure 23. Total strain energy density as the fatigue damage parameter at different strain amplitudes along different directions for ZK60 extrusion

6. Conclusions

This study explored the mechanical behavior of ZK60 extrusion Mg alloy in three different directions: extrusion (ED), radial (RD), and 45°. From the results and discussions, the following conclusions can be made:

- The extruded alloy exhibited a sharp basal texture in the microstructure such that the hexagonal crystals were randomly orientated with their c-axes perpendicular to the extrusion direction.
- The quasi-static behavior of ZK60 extrusion depended on the material's direction in the light of the developed texture. Indeed, while the static behavior along ED was asymmetric in tension and compression, the RD and 45° samples exhibited symmetric behaviors.
- In spite of dissimilar quasi-static behaviors along the different directions, the cyclic behavior in the LCF regime was not sensitive to the direction. However, the behaviors in the HCF regime were distinct.
- JV, as an energy-based model, provides acceptable fatigue life predictions for ZK60 extrusion with anisotropic behavior.

References

[1] H. Friedrich and S. Schumann, "Research for a 'new age of magnesium' in the automotive industry," *J. Mater. Process. Technol.*, vol. 117, no. 3, pp. 276–281, 2001.

[2] M. K. Kulekci, "Magnesium and its alloys applications in automotive industry," *Int. J. Adv. Manuf. Technol.*, vol. 39, no. 9–10, pp. 851–865, Nov. 2008.

[3] M. M. Avedesian and H. Baker, *ASM specialty handbook: magnesium and magnesium alloys*. 1999.

[4] G. Liu, R. Xin, F. Liu, and Q. Liu, "Twinning characteristic in tension of magnesium alloys and its effect on mechanical properties," *Mater. Des.*, vol. 107, pp. 503–510, 2016.

[5] F. Mokdad, D. L. Chen, and D. Y. Li, "Single and double twin nucleation, growth, and interaction in an extruded magnesium alloy," *Mater. Des.*, vol. 119, pp. 376–396, 2017.

[6] E. I. Galindo-Nava, "Modelling twinning evolution during plastic deformation in hexagonal close-packed metals," *Mater. Des.*, vol. 83, pp. 327–343, 2015.

[7] F. A. Mirza, D. L. Chen, D. J. Li, and X. Q. Zeng, "Low cycle fatigue of an extruded Mg-3Nd-0.2Zn-0.5Zr magnesium alloy," *Mater. Des.*, vol. 64, pp. 63–73, 2014.

[8] F. Mokdad and D. L. Chen, "Strain-controlled low cycle fatigue properties of a rare-earth containing ZEK100 magnesium alloy," *Mater. Des.*, vol. 67, pp. 436–447, 2015.

[9] S. H. Park, S. G. Hong, W. Bang, and C. S. Lee, "Effect of anisotropy on the low-cycle fatigue behavior of rolled AZ31 magnesium alloy," *Mater. Sci. Eng. A*, vol. 527, no. 3, pp. 417–423, 2010.

[10] F. Lv *et al.*, "Fatigue properties of rolled magnesium alloy (AZ31) sheet: Influence of specimen orientation," *Int. J. Fatigue*, vol. 33, no. 5, pp. 672–682, 2011.

[11] S. Ishihara, S. Taneguchi, H. Shibata, T. Goshima, and a. Saiki, "Anisotropy of the fatigue behavior of extruded and rolled magnesium alloys," *Int. J. Fatigue*, vol. 50, pp. 94–100, 2013.

[12] J. Dallmeier, O. Huber, H. Saage, and K. Eigenfeld, "Uniaxial cyclic deformation and fatigue behavior of AM50 magnesium alloy sheet metals under symmetric and asymmetric loadings," *Mater. Des.*, vol. 70, pp. 10–30, 2015.

[13] Z. Bin Sajuri, Y. Miyashita, Y. Hosokai, and Y. Mutoh, "Effects of Mn content and texture on fatigue properties of as-cast and extruded AZ61 magnesium alloys," *Int. J. Mech. Sci.*, vol. 48, no. 2, pp. 198–209, 2006.

[14] J. B. Jordon *et al.*, "Investigation of fatigue anisotropy in an extruded magnesium alloy," *Int. J. Fatigue*, vol. 51, pp. 8–14, 2013.

[15] A. A. Roostaei and H. Jahed, "Role of loading direction on cyclic behaviour characteristics of AM30 extrusion and its fatigue damage modelling," *Mater. Sci. Eng. A*, vol. 670, pp. 26–40, 2016.

[16] C. Wang, T. J. Luo, J. X. Zhou, and Y. S. Yang, "Anisotropic cyclic deformation behavior of extruded ZA81M magnesium alloy," *Int. J. Fatigue*, vol. 96, pp. 178–184, 2017.

[17] Y. Xiong and Y. Jiang, "Cyclic deformation and fatigue of rolled AZ80 magnesium alloy along different material orientations," *Mater. Sci. Eng. A*, vol. 677, pp. 58–67, 2016.

[18] H. T. Zhou, Z. D. Zhang, C. M. Liu, and Q. W. Wang, "Effect of Nd and Y on the microstructure and mechanical properties of ZK60 alloy," *Mater. Sci. Eng. A*, vol. 445–446, pp. 1–6, 2007.

[19] Y. Xiong and Y. Jiang, "Fatigue of ZK60 magnesium alloy under uniaxial loading," *Int. J. Fatigue*, vol. 64, pp. 74–83, 2014.

[20] Y. Xiong, Q. Yu, and Y. Jiang, "An experimental study of cyclic plastic deformation of extruded ZK60 magnesium alloy under uniaxial loading at room temperature," *Int. J. Plast.*, vol. 53, pp. 107–124, 2014.
[21] Q. Yu, J. Zhang, Y. Jiang, and Q. Li, "An experimental study on cyclic deformation and fatigue of extruded ZK60 magnesium alloy," *Int. J. Fatigue*, vol. 36, no. 1, pp. 47–58, 2012.
[22] L. Wu *et al.*, "Twinning-detwinning behavior during the strain-controlled low-cycle fatigue testing of a wrought magnesium alloy, ZK60A," *Acta Mater.*, vol. 56, no. 4, pp. 688–695, 2008.
[23] Y. Xiong, Q. Yu, and Y. Jiang, "Deformation of extruded ZK60 magnesium alloy under uniaxial loading in different material orientations," *Mater. Sci. Eng. A*, vol. 710, no. July 2017, pp. 206–213, 2018.
[24] M. W. Brown and K. J. Miller, "A Theory for Fatigue Failure under Multiaxial Stress-Strain Conditions," *Proc. Inst. Mech. Eng.*, vol. 187, no. 1, pp. 745–755, 1973.
[25] Y. Y. Wang and W. X. Yao, "Evaluation and comparison of several multiaxial fatigue criteria," *Int. J. Fatigue*, vol. 26, no. 1, pp. 17–25, 2004.
[26] A. Carpinteri and A. Spagnoli, "Multiaxial high-cycle fatigue criterion for hard metals," *Int. J. Fatigue*, vol. 23, no. 2, pp. 135–145, 2001.
[27] A. Varvani-Farahani, "New energy-critical plane parameter for fatigue life assessment of various metallic materials subjected to in-phase and out-of-phase multiaxial fatigue loading conditions," *Int. J. Fatigue*, vol. 22, no. 4, pp. 295–305, 2000.
[28] E. Macha and C. M. Sonsino, "Energy criteria of multiaxial fatigue failure," *Fatigue Fract. Eng. Mater. Struct.*, vol. 22, no. 12, pp. 1053–1070, 1999.
[29] I. Papadopoulos, "A comparative study of multiaxial high-cycle fatigue criteria for metals," *Int. J. Fatigue*, vol. 19, no. 3, pp. 219–235, 1997.
[30] D. Socie, "Critical plane approaches for multiaxial fatigue damage assessment," *ASTM Spec. Tech. Publ.*, vol. 1191, pp. 7–36, 1993.
[31] J. A. Bannantine, "A review of mutiaxial fatigue damage model and observed material behavior," pp. 213–237, 1991.
[32] K. Lieb *et al.*, "Multiaxial Fatigue: A Survey of the State of the Art," *J. Test. Eval.*, vol. 9, no. 3, p. 165, 1981.
[33] E. Krempl, *The Influence of State of Stress on Low-Cycle Fatigue of Structural Materials. A Literature Survey and Interpretive Report*. 1974.
[34] S. Zheng, Q. Yu, and Y. Jiang, "An experimental study of fatigue crack propagation in extruded AZ31B magnesium alloy," *Int. J. Fatigue*, vol. 47, pp. 174–183, 2013.
[35] H. Jahed and A. Varvani-Farahani, "Upper and lower fatigue life limits model using energy-based fatigue properties," *Int. J. Fatigue*, vol. 28, no. 5–6, pp. 467–473, 2006.
[36] S. M. H. Karparvarfard, S. K. Shaha, S. B. Behravesh, H. Jahed, and B. W. Williams, "Fatigue characteristics and modeling of cast and cast-forged ZK60 magnesium alloy," *Int. J. Fatigue*, no. November 2017, pp. 1–15, 2018.
[37] H. Jahed, A. Varvani-Farahani, M. Noban, and I. Khalaji, "An energy-based fatigue life assessment model for various metallic materials under proportional and non-proportional loading conditions," *Int. J. Fatigue*, vol. 29, no. 4, pp. 647–655, 2007.
[38] Y. S. Garud, "A New Approach to the Evaluation of Fatigue Under Multiaxial Loadings," *J. Eng. Mater. Technol.*, vol. 103, no. 2, p. 118, 1981.
[39] J. Albinmousa, H. Jahed, and S. Lambert, "Cyclic behaviour of wrought magnesium alloy under multiaxial load," *Int. J. Fatigue*, vol. 33, no. 8, pp. 1127–1139, 2011.
[40] Kn. Smith, T. H. Topper, and P. Watson, "A stress-strain function for the fatigue of

metals(Stress-strain function for metal fatigue including mean stress effect)," *J. Mater.*, vol. 5, no. January 1970, pp. 767–778, 1970.

[41] D. Toscano, S. K. Shaha, B. Behravesh, H. Jahed, and B. Williams, "Effect of forging on the low cycle fatigue behavior of cast AZ31B alloy," *Mater. Sci. Eng. A*, vol. 706, no. August, pp. 342–356, 2017.

[42] ASTM and ASTM Int., "Standard Test Methods for Tension Testing of Metallic Materials 1," *Astm*, no. C, pp. 1–27, 2016.

[43] Y. Xiong, X. Gong, and Y. Jiang, "Effect of initial texture on fatigue properties of extruded ZK60 magnesium alloy," *Fatigue Fract. Eng. Mater. Struct.*, vol. 274–276, no. I, pp. 193–198, Feb. 2018.

[44] D. W. Brown, A. Jain, S. R. Agnew, and B. Clausen, "Twinning and Detwinning during Cyclic Deformation of Mg Alloy AZ31B," *Mater. Sci. Forum*, vol. 539–543, pp. 3407–3413, 2007.

[45] S. R. Agnew and and J. J. B. Christopher A. Calhoun, "What is in a Strain Hardening 'Plateau'?," in *Magnesium Technology 2016, Springer International Publishing*, 2016, pp. 189–194.

[46] N. a. Fleck, G. M. Muller, M. F. Ashby, and J. W. Hutchinson, "Strain gradient plasticity: Theory and experiment," *Acta Metall. Mater.*, vol. 42, no. 2, pp. 475–487, 1994.

[47] K. Máthis, P. Beran, J. Čapek, P. Lukáš, and P. Lukáš, "In-situ neutron diffraction and acoustic emission investigation of twinning activity in magnesium," *J. Phys. Conf. Ser.*, vol. 340, no. 1, p. 12096, 2012.

[48] G. Proust, C. N. Tomé, A. Jain, and S. R. Agnew, "Modeling the effect of twinning and detwinning during strain-path changes of magnesium alloy AZ31," *Int. J. Plast.*, vol. 25, no. 5, pp. 861–880, 2009.

[49] Q. Yu, J. Zhang, and Y. Jiang, "Fatigue damage development in pure polycrystalline magnesium under cyclic tension-compression loading," *Mater. Sci. Eng. A*, vol. 528, no. 25–26, pp. 7816–7826, 2011.

[50] S. M. H. H. Karparvarfard, S. K. Shaha, S. B. Behravesh, H. Jahed, and B. W. Williams, "Microstructure, texture and mechanical behavior characterization of hot forged cast ZK60 magnesium alloy," *J. Mater. Sci. Technol.*, vol. 33, no. 9, pp. 907–918, 2017.

[51] H. Yu, Y. Xin, A. Chapuis, X. Huang, R. Xin, and Q. Liu, "The different effects of twin boundary and grain boundary on reducing tension-compression yield asymmetry of Mg alloys," *Nat. Publ. Gr.*, no. May, pp. 4–11, 2016.

[52] Y. J. Wu, R. Zhu, J. T. Wang, and W. Q. Ji, "Role of twinning and slip in cyclic deformation of extruded Mg-3%Al-1%Zn alloys," *Scr. Mater.*, vol. 63, no. 11, pp. 1077–1080, 2010.

[53] F. Yang, S. M. Yin, S. X. Li, and Z. F. Zhang, "Crack initiation mechanism of extruded AZ31 magnesium alloy in the very high cycle fatigue regime," *Mater. Sci. Eng. A*, vol. 491, no. 1–2, pp. 131–136, 2008.

[54] J. Albinmousa and H. Jahed, "Multiaxial effects on LCF behaviour and fatigue failure of AZ31B magnesium extrusion," *Int. J. Fatigue*, vol. 67, pp. 103–116, 2014.

[55] F. Castro and Y. Jiang, "Fatigue life and early cracking predictions of extruded AZ31B magnesium alloy using critical plane approaches," *Int. J. Fatigue*, vol. 88, pp. 236–246, 2016.

[56] S. H. Park, S. G. Hong, J. Yoon, and C. S. Lee, "Influence of loading direction on the anisotropic fatigue properties of rolled magnesium alloy," *Int. J. Fatigue*, vol. 87, pp. 210–215, 2016.

[57] F. Castro and Y. Jiang, "Fatigue of extruded AZ31B magnesium alloy under stress- and

strain-controlled conditions including step loading," *Mech. Mater.*, vol. 108, pp. 77–86, 2017.

[58] A. Gryguc, S. K. Shaha, H. Jahed, M. Wells, B. Williams, and J. McKinley, "Tensile and fatigue behaviour of as-forged AZ31B extrusion," *Frat. ed Integrita Strutt.*, vol. 10, no. 38, pp. 251–258, 2016.

Author Contributions Section

All authors have been involved in the study, experiments, data analysis, and writing of the manuscript. Following are the roles of each of the authors in this study.

1. AH. Pahlevanpour, SMH. Karparvarfard, Graduate Students: performed all quasi-static and cyclic tests in extrusion, radial and 45 directions, analyzed the data, and developed the fatigue model based on single set of properties.
2. S.K. Shaha, S.B. Behravesh, Postdoctoral Fellows: performed texture and fracture analysis, developed the microstructural link to fatigue behavior in the three directions and helped with the fatigue modeling development.
3. S. Adibnazari and H. Jahed, co-supervisors: conceptualized the study, guided the material characterization and fatigue modeling analysis.

All authors have read and agreed with the content of the manuscript.

Highlights

- Quasi-static behavior along extrusion direction is tension-compression asymmetry; whereas, radial and 45° directions showed symmetric behaviors.
- Fatigue response of as-extruded ZK60 is not sensitive to the material direction in the low cycle fatigue regime.
- Extrusion direction exhibits higher fatigue life in comparison to the radial and 45° directions in the high cycle fatigue regime.
- Twin lamellae in extrusion direction, and slip bands in radial direction were dominant features of the fracture surfaces.
- The Jahed-Varvani fatigue model predicts the fatigue life along all the directions with a single set of material parameters.

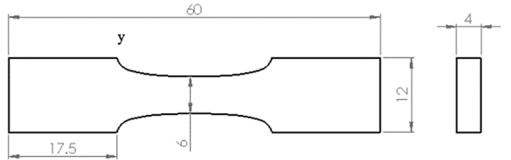
60
y
4
12
6
17.5
(a)

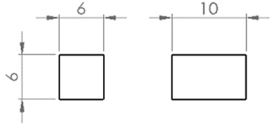
6
10
6
(b)

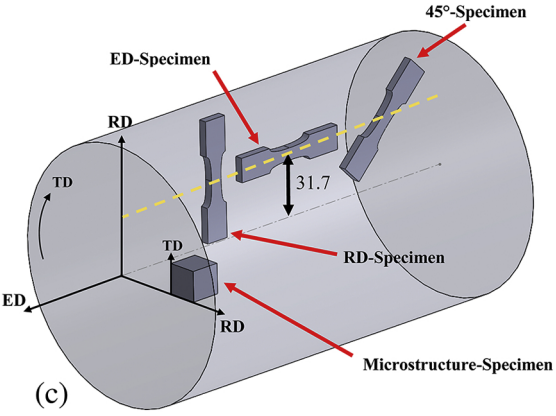
45°-Specimen
ED-Specimen
RD
TD
31.7
TD
RD-Specimen
ED
RD
Microstructure-Specimen
(c)

Figure 1

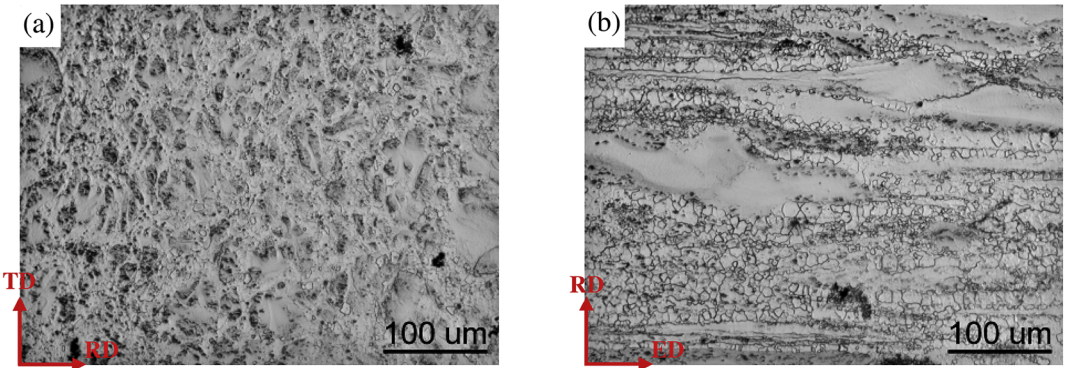

Figure 2

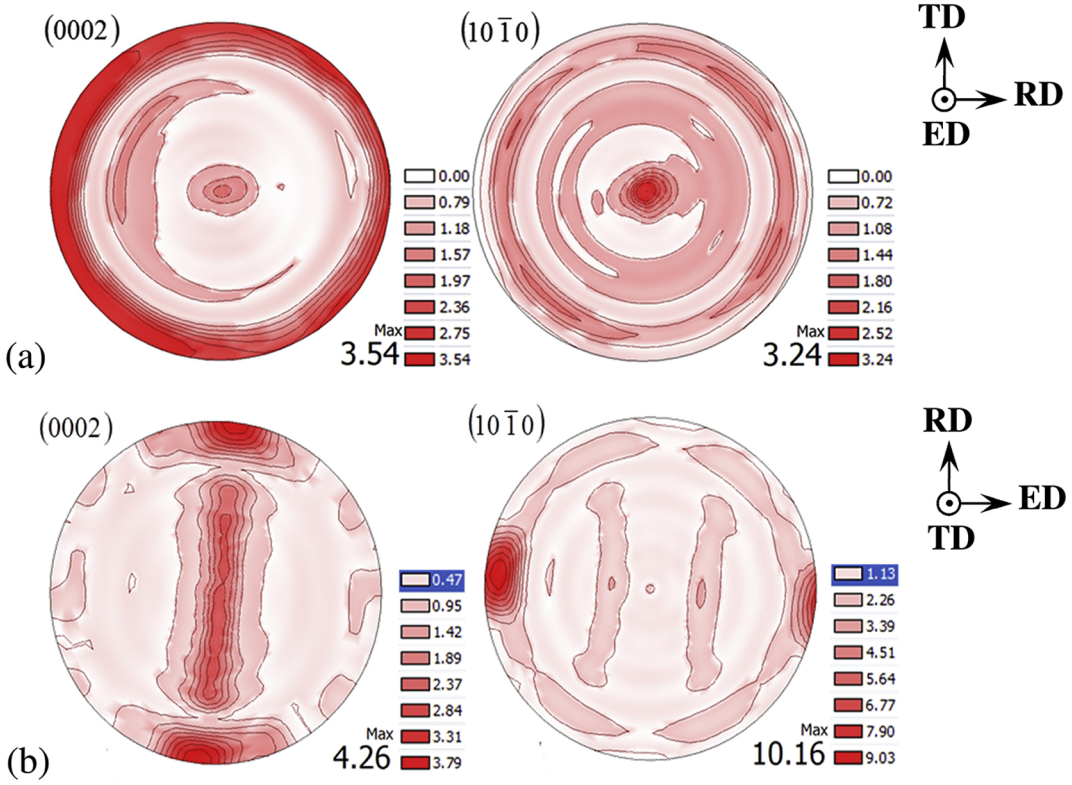
(0002)
(10$\bar{1}$0)
TD
RD
ED
0.00
0.79
1.18
1.57
1.97
2.36
Max
2.75
3.54
3.54
0.00
0.72
1.08
1.44
1.80
2.16
Max
2.52
3.24
3.24
(a)
(0002)
(10$\bar{1}$0)
RD
ED
TD
0.47
0.95
1.42
1.89
2.37
2.84
Max
3.31
4.26
3.79
1.13
2.26
3.39
4.51
5.64
6.77
Max
7.90
10.16
9.03
(b)

Figure 3

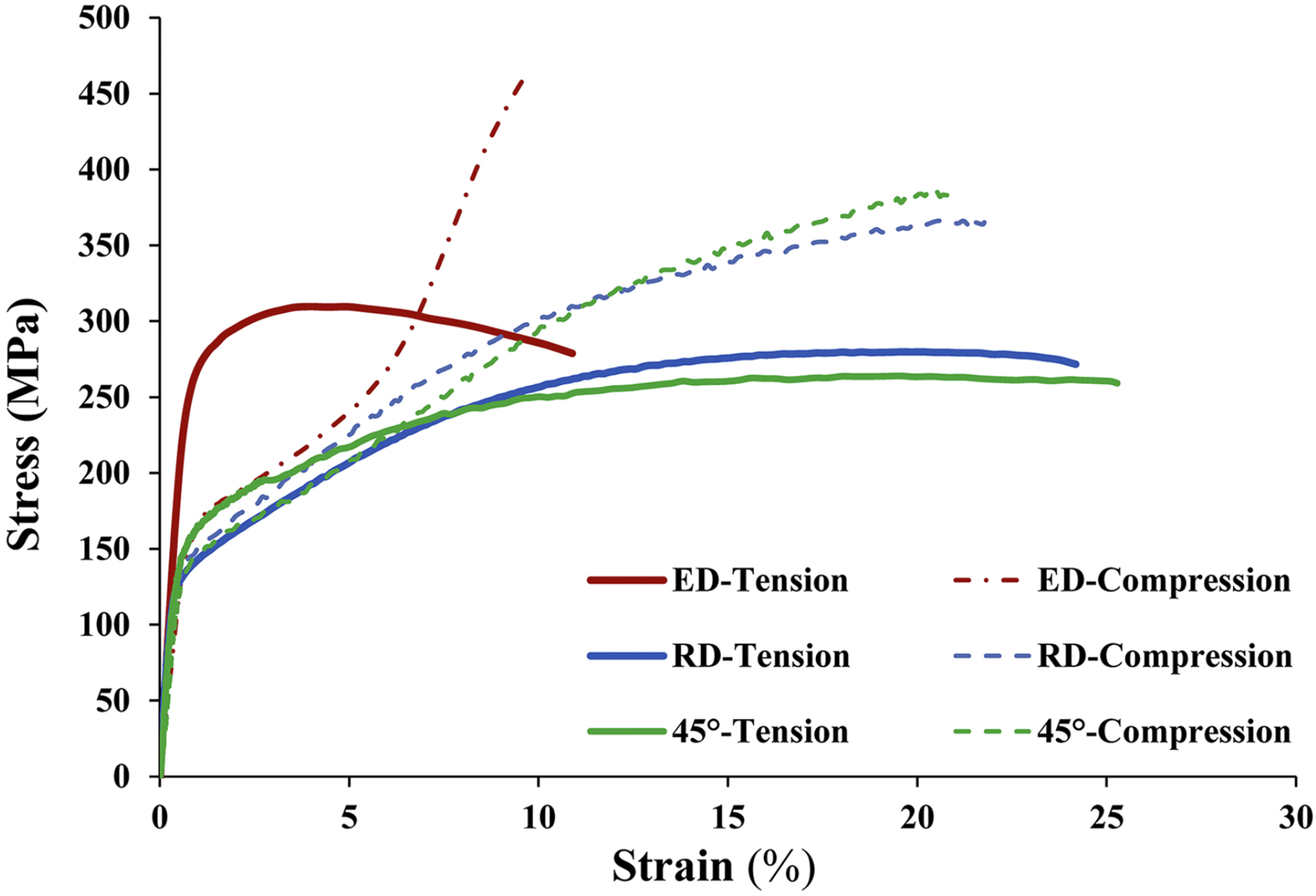
Stress (MPa)
500
450
400
350
300
250
200
150
100
50
0
0
5
10
15
20
25
30
Strain (%)
ED-Tension
ED-Compression
RD-Tension
RD-Compression
45°-Tension
45°-Compression

Figure 4

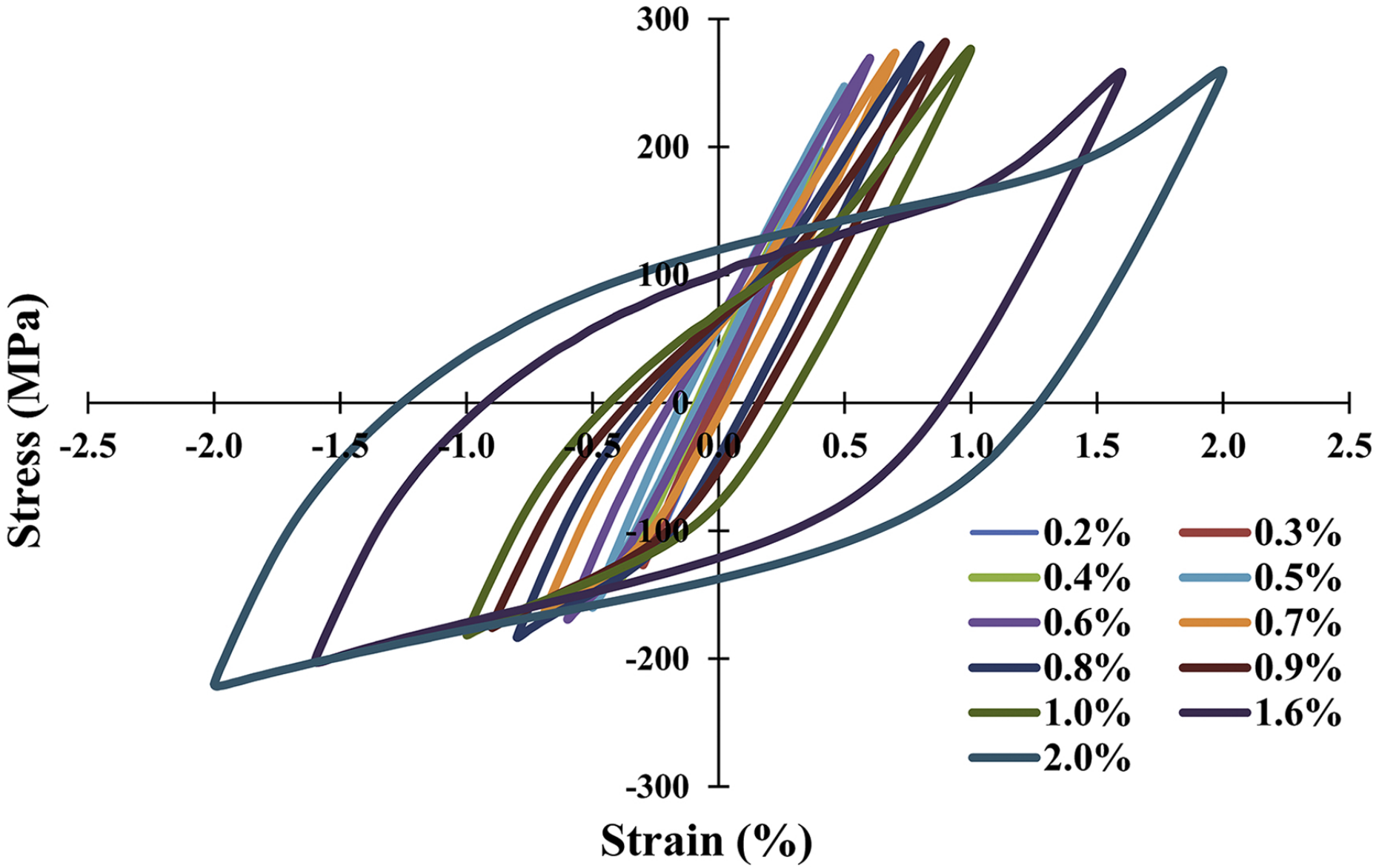
300
200
100
0
-100
-200
-300
-2.5
-2.0
-1.5
-1.0
-0.5
0.0
0.5
1.0
1.5
2.0
2.5
Stress (MPa)
Strain (%)
0.2%
0.3%
0.4%
0.5%
0.6%
0.7%
0.8%
0.9%
1.0%
1.6%
2.0%

Figure 5

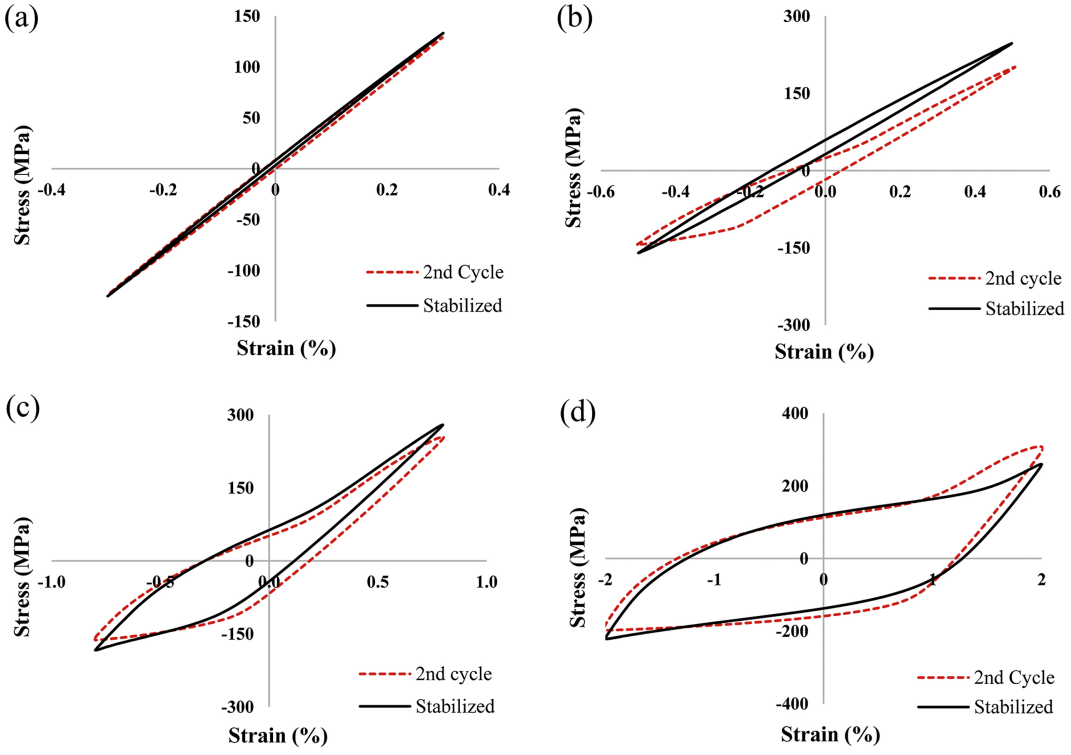
(a)
Stress (MPa)
Strain (%)
2nd Cycle
Stabilized
(b)
Stress (MPa)
Strain (%)
2nd cycle
Stabilized
(c)
Stress (MPa)
Strain (%)
2nd cycle
Stabilized
(d)
Stress (MPa)
Strain (%)
2nd Cycle
Stabilized

Figure 6

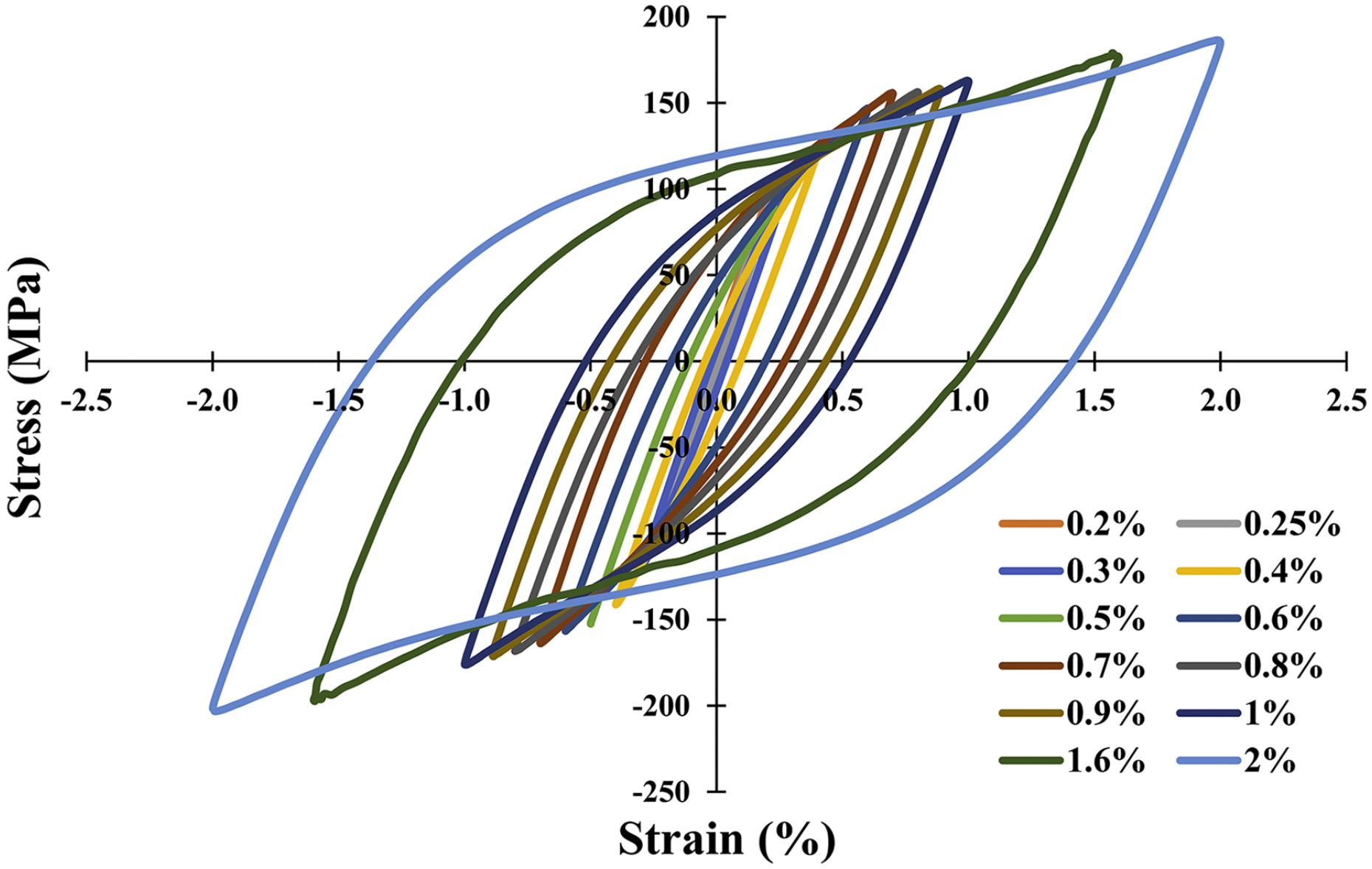
Stress (MPa)
200
150
100
50
0
-50
-100
-150
-200
-250
-2.5
-2.0
-1.5
-1.0
-0.5
0.0
0.5
1.0
1.5
2.0
2.5
Strain (%)
0.2%
0.25%
0.3%
0.4%
0.5%
0.6%
0.7%
0.8%
0.9%
1%
1.6%
2%

Figure 7

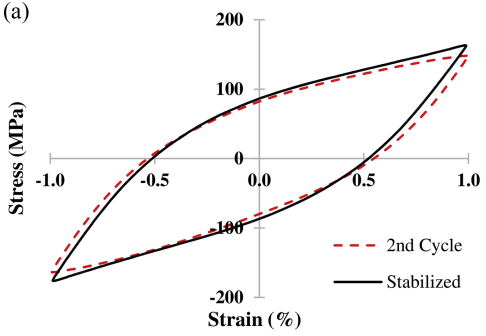
(a)
200
100
0
-100
-200
-1.0
-0.5
0.0
0.5
1.0
Stress (MPa)
Strain (%)
2nd Cycle
Stabilized

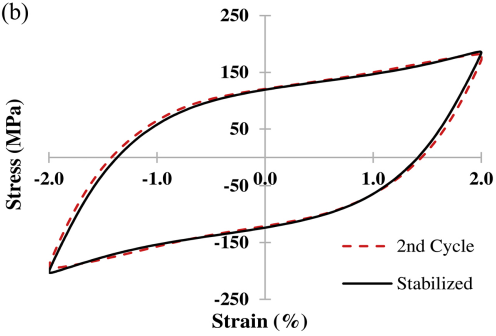
(b)
250
150
50
-50
-150
-250
-2.0
-1.0
0.0
1.0
2.0
Stress (MPa)
Strain (%)
2nd Cycle
Stabilized

Figure 8

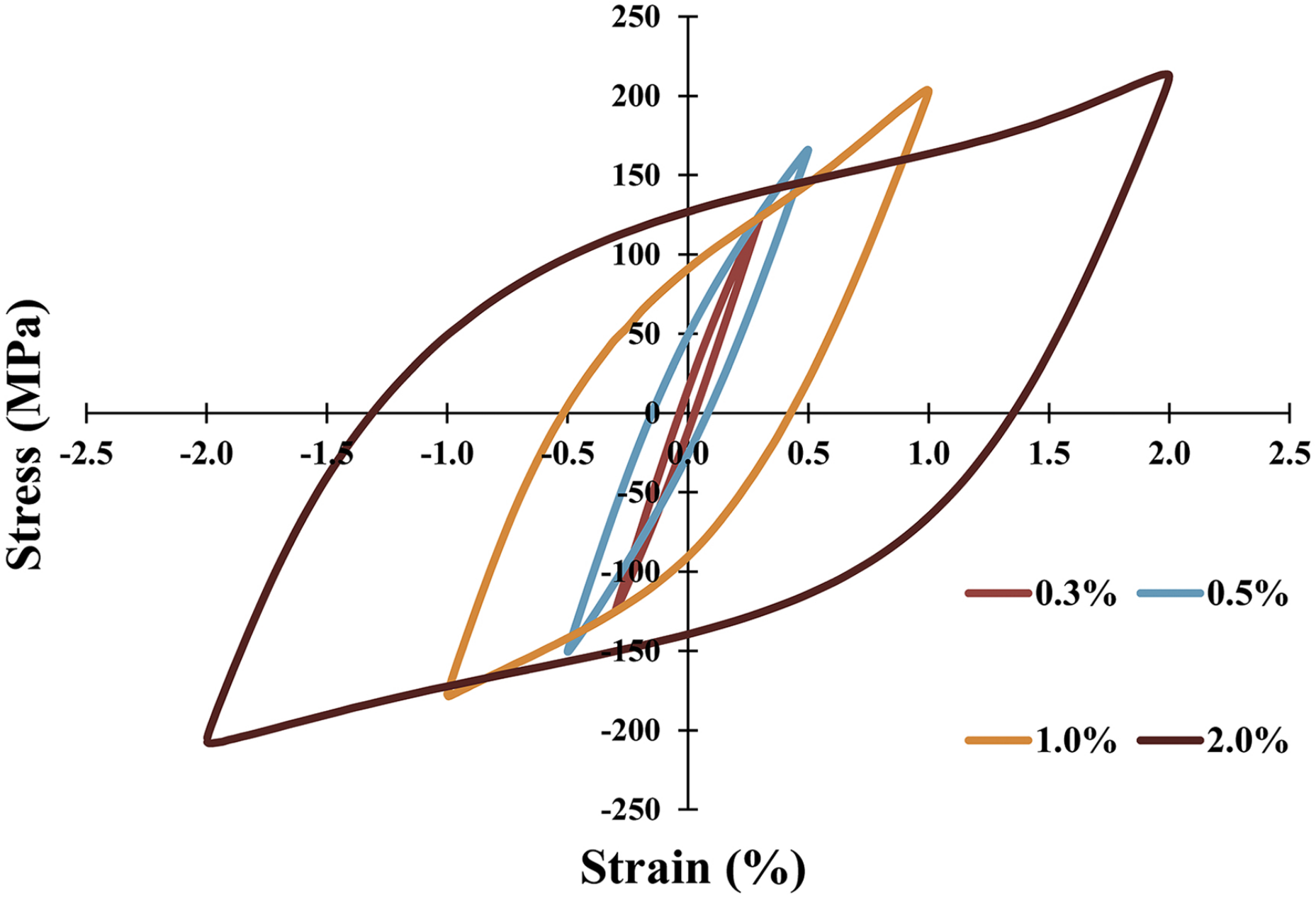
250
200
150
100
50
0
-50
-100
-150
-200
-250
-2.5
-2.0
-1.5
-1.0
-0.5
0.0
0.5
1.0
1.5
2.0
2.5
Stress (MPa)
Strain (%)
0.3%
0.5%
1.0%
2.0%

Figure 9

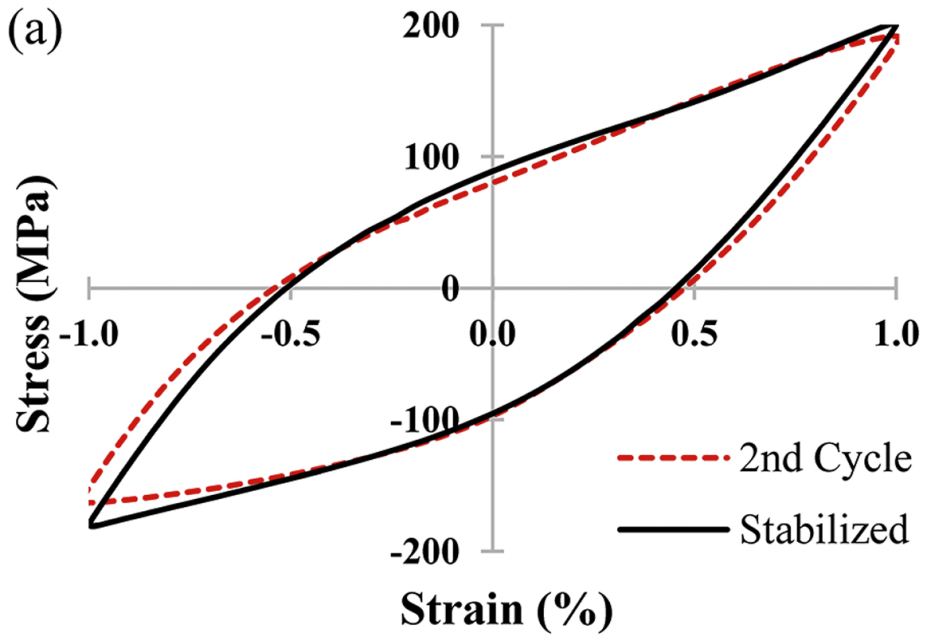
(a)
200
100
0
-100
-200
-1.0
-0.5
0.0
0.5
1.0
Stress (MPa)
Strain (%)
2nd Cycle
Stabilized

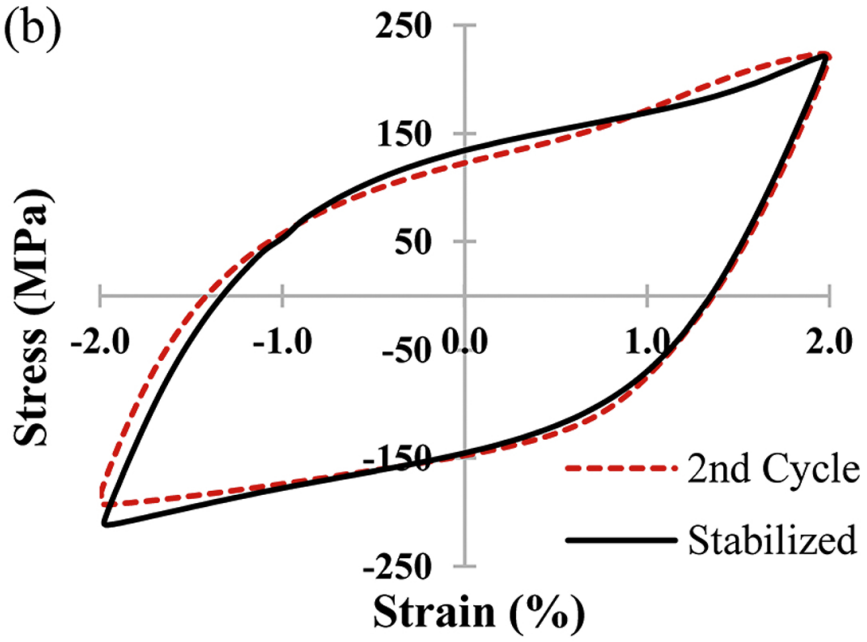
(b)
250
150
50
-50
-150
-250
-2.0
-1.0
0.0
1.0
2.0
Stress (MPa)
Strain (%)
2nd Cycle
Stabilized

Figure 10

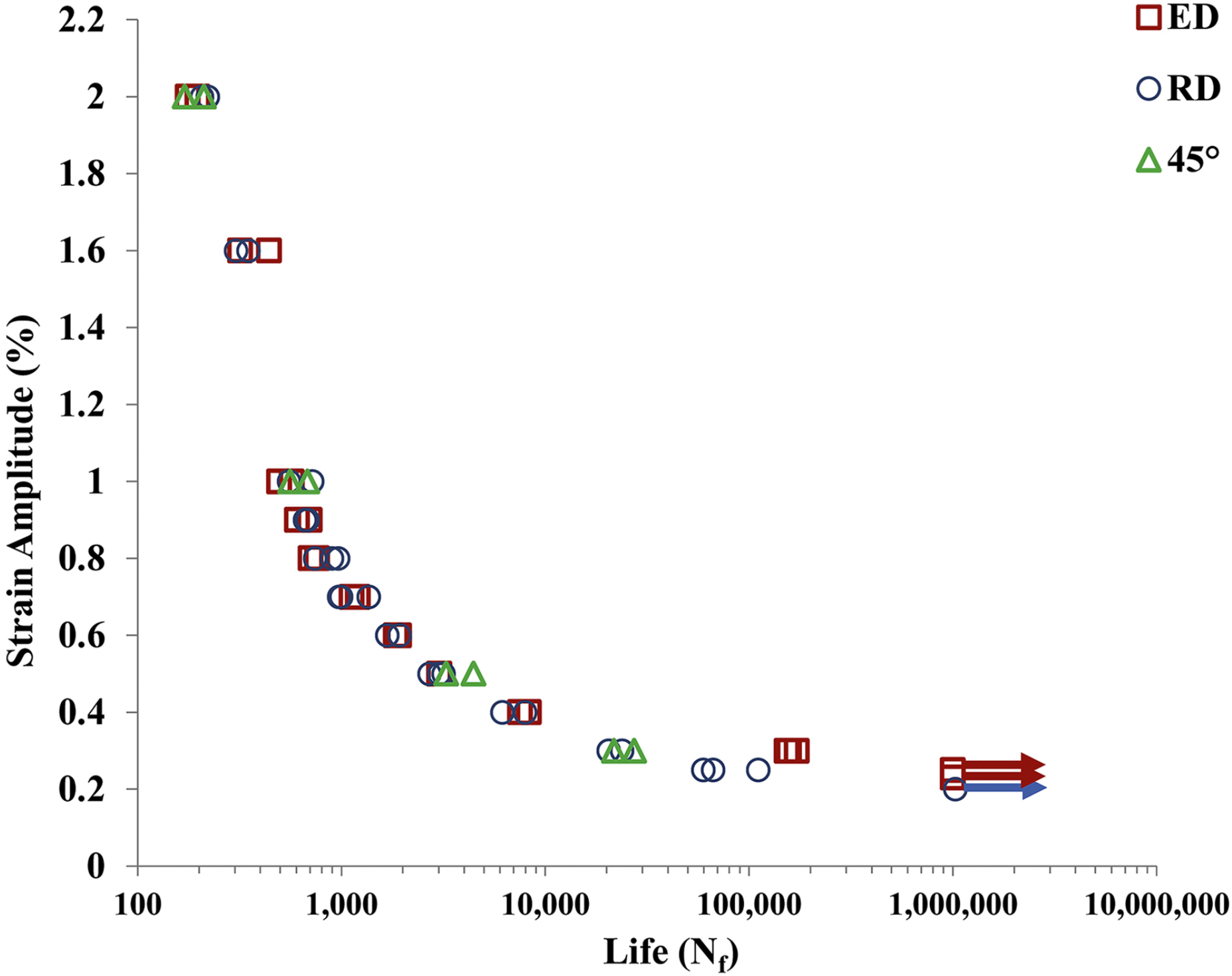
ED
RD
45°
Strain Amplitude (%)
2.2
2
1.8
1.6
1.4
1.2
1
0.8
0.6
0.4
0.2
0
100
1,000
10,000
100,000
1,000,000
10,000,000
Life (N_f)

Figure 11

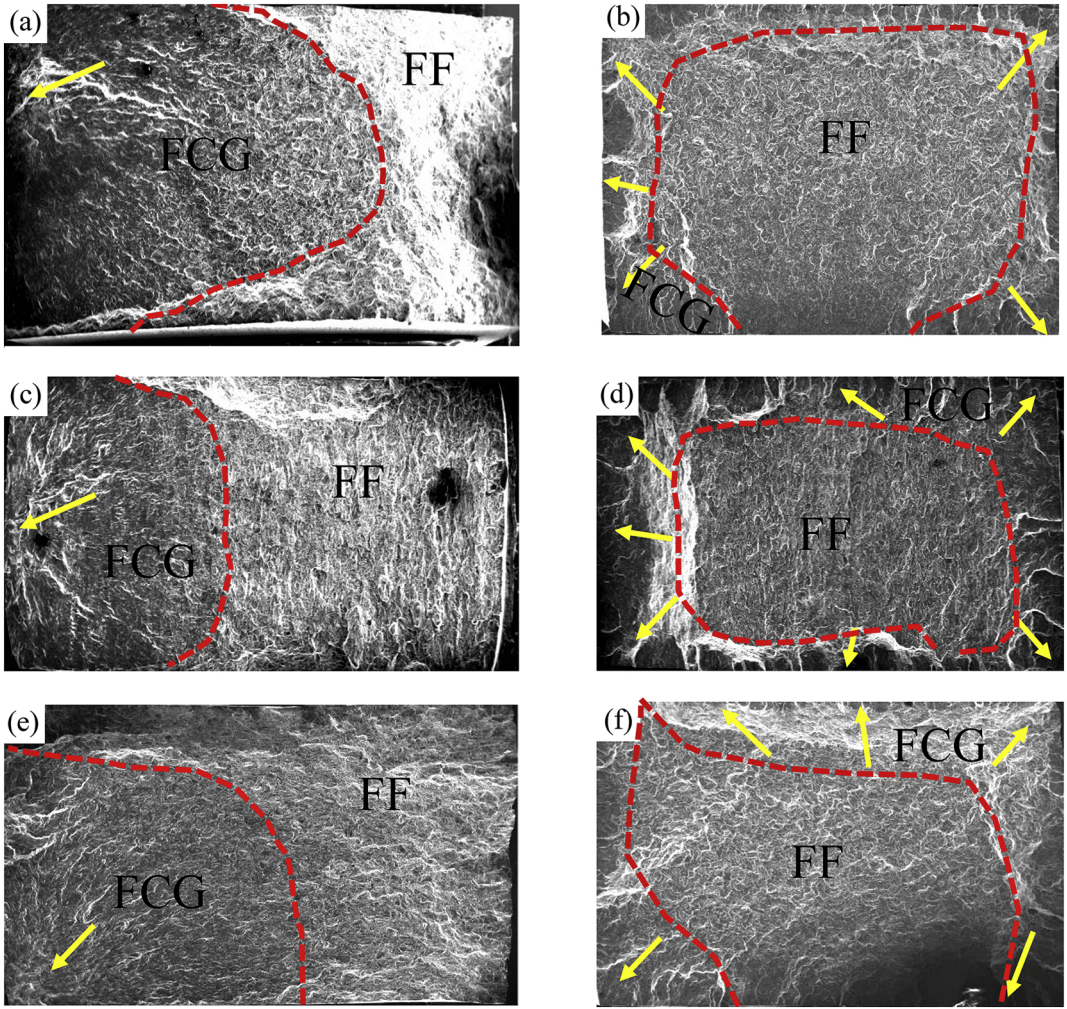

Figure 12

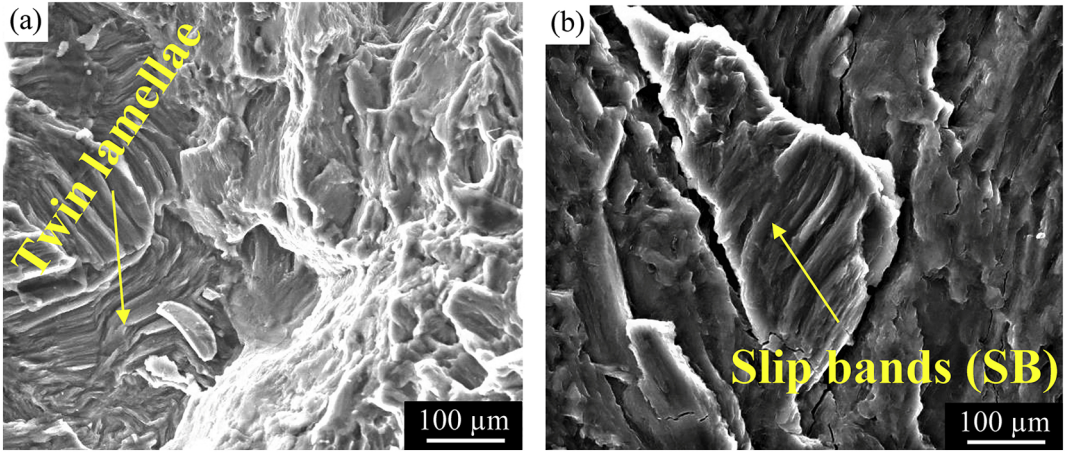

Figure 13

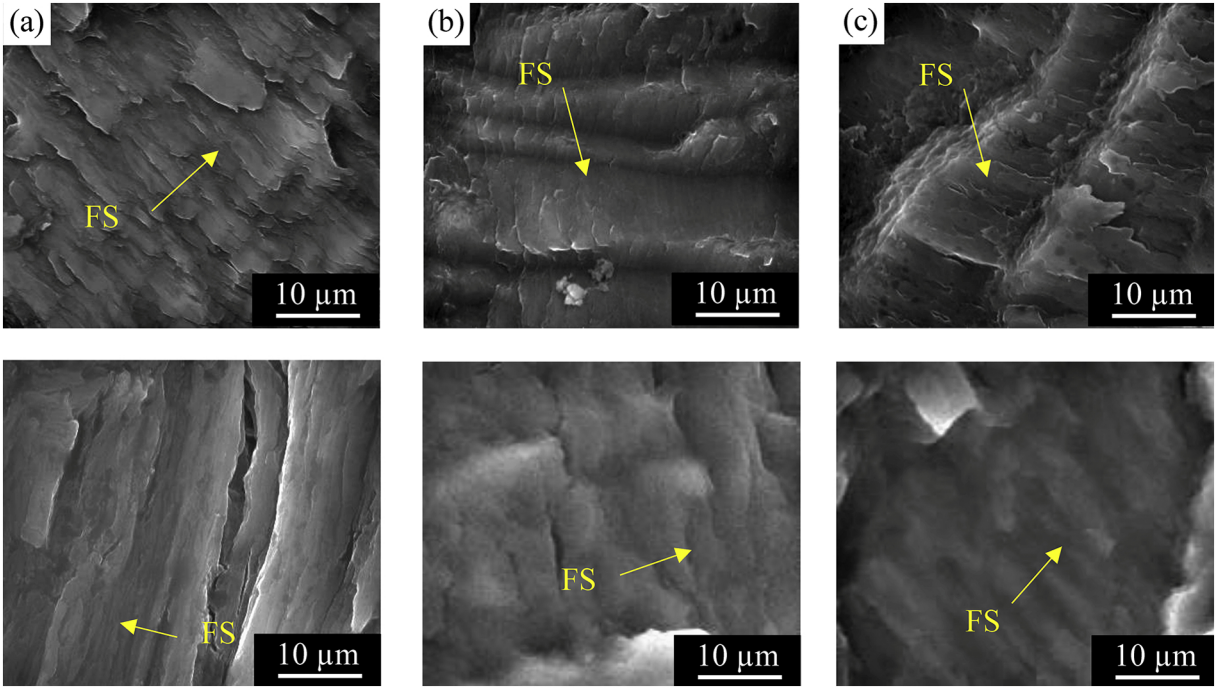

Figure 14

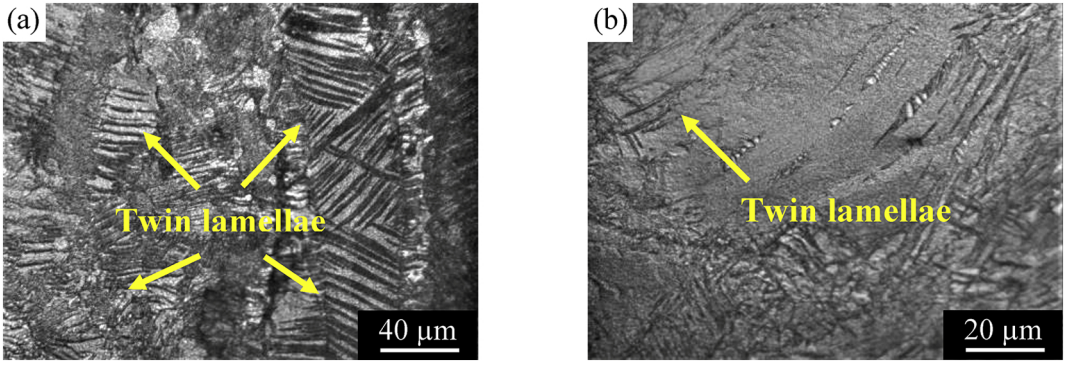

Figure 15

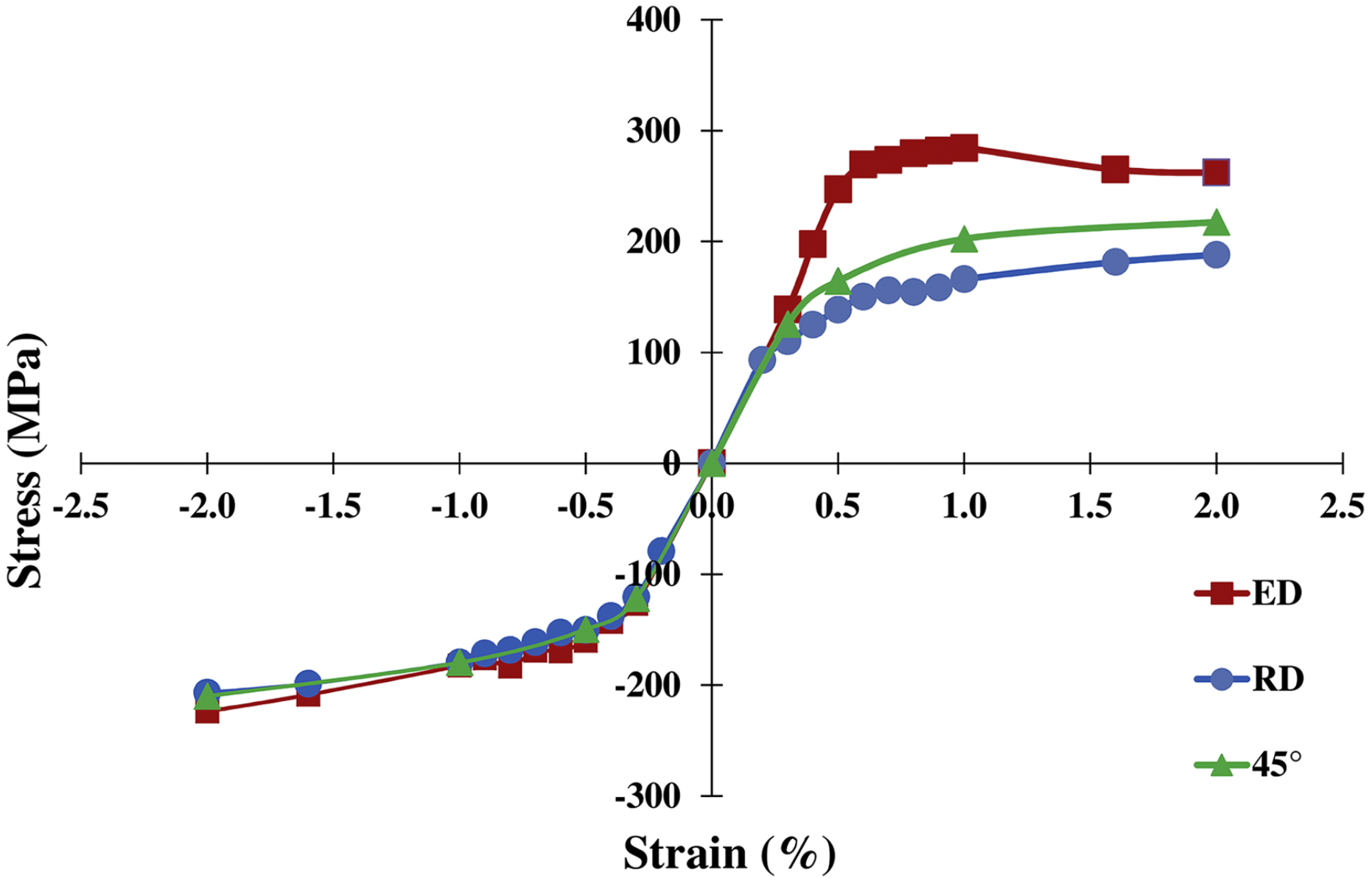
400
300
200
100
0
-100
-200
-300
-2.5
-2.0
-1.5
-1.0
-0.5
0.0
0.5
1.0
1.5
2.0
2.5
Stress (MPa)
Strain (%)
ED
RD
45°

Figure 16

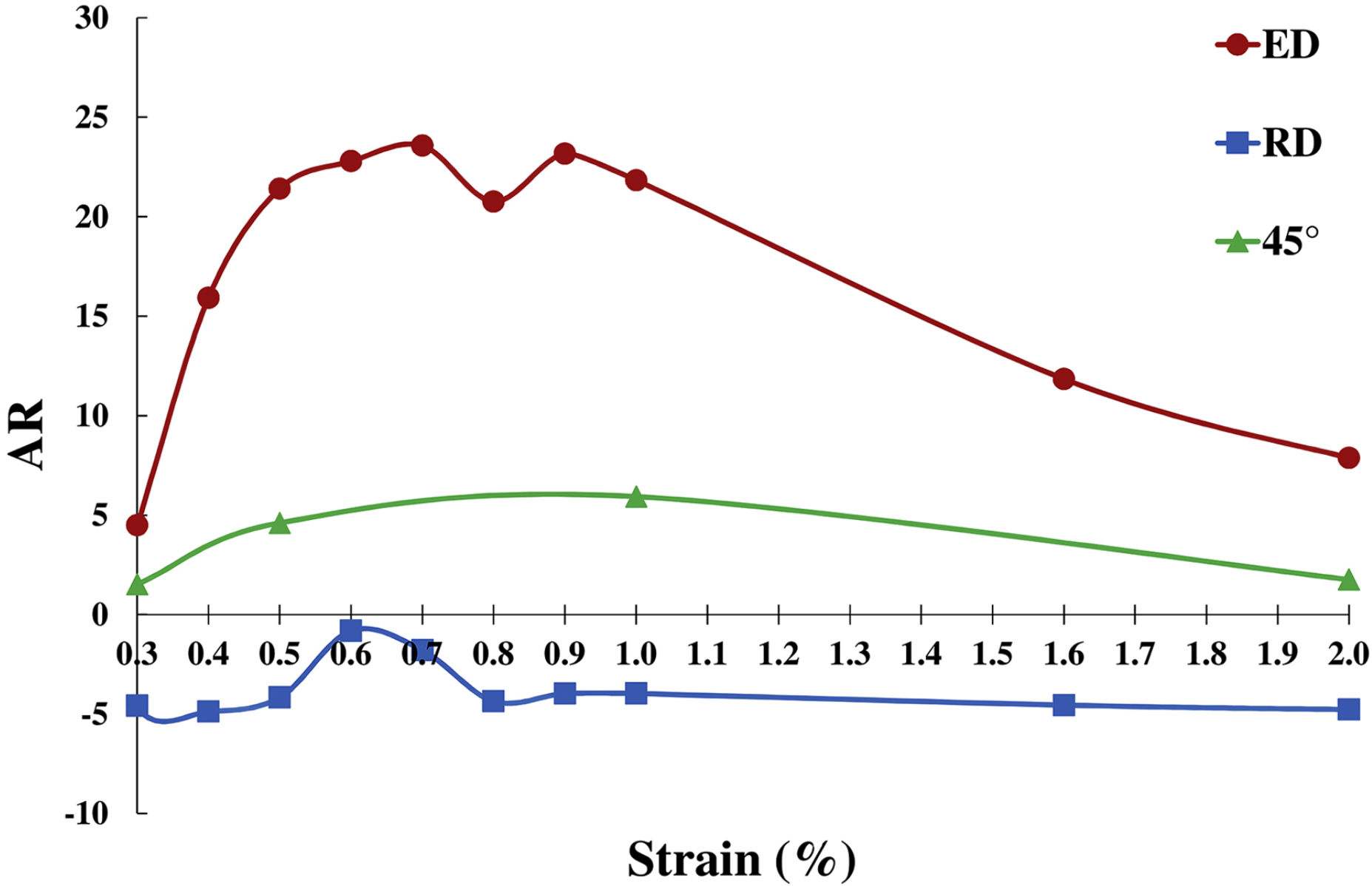
30
25
20
15
10
5
0
-5
-10
AR
0.3
0.4
0.5
0.6
0.7
0.8
0.9
1.0
1.1
1.2
1.3
1.4
1.5
1.6
1.7
1.8
1.9
2.0
Strain (%)
ED
RD
45°

Figure 17

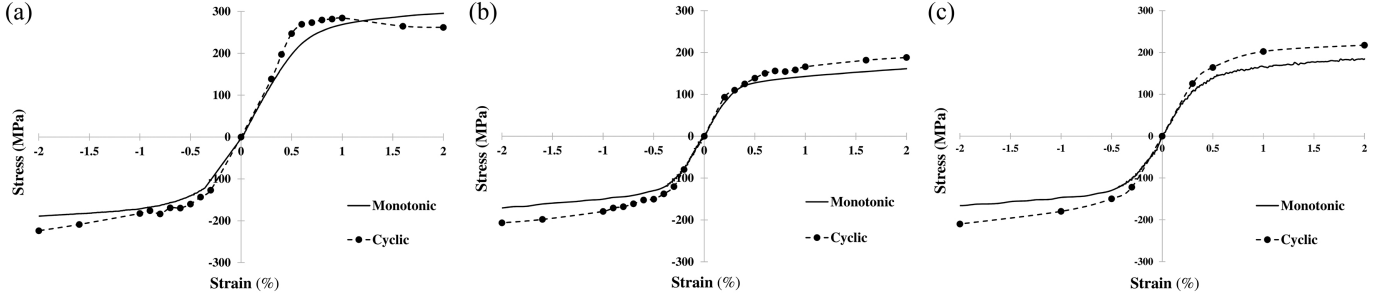
(a)
(b)
(c)
Stress (MPa)
Strain (%)
Monotonic
Cyclic
300
200
100
0
-100
-200
-300
-2
-1.5
-1
-0.5
0
0.5
1
1.5
2

Figure 18

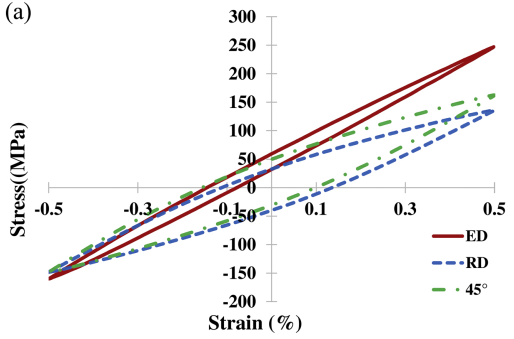

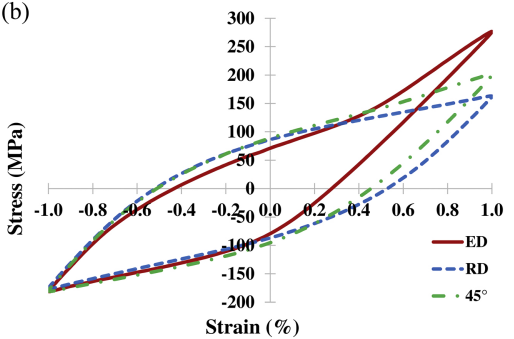

Figure 19

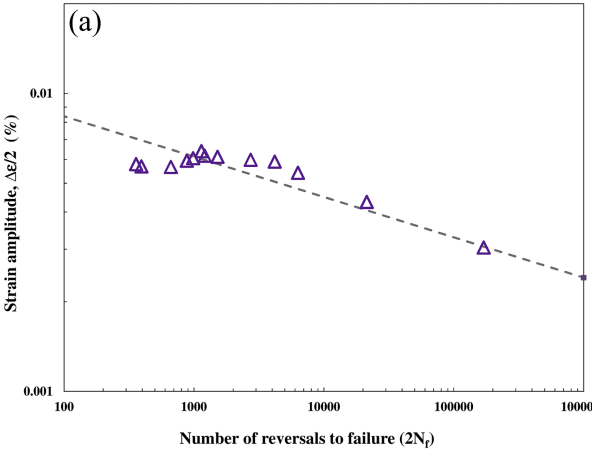
(a)
0.01
0.001
Strain amplitude, Δε/2 (%)
100
1000
10000
100000
1000000
Number of reversals to failure (2N_f)

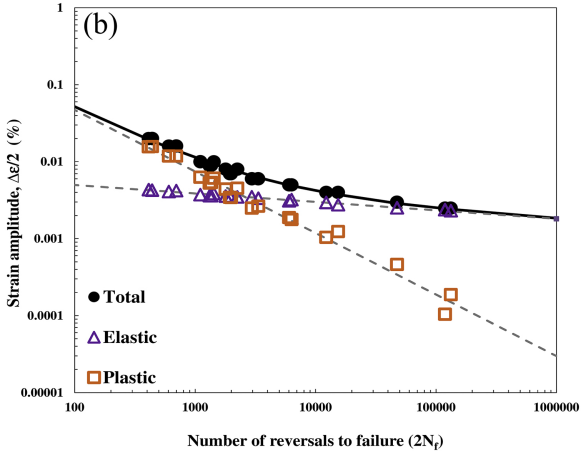
(b)
1
0.1
0.01
0.001
0.0001
0.00001
Strain amplitude, Δε/2 (%)
Total
Elastic
Plastic
100
1000
10000
100000
1000000
Number of reversals to failure (2N_f)

Figure 20

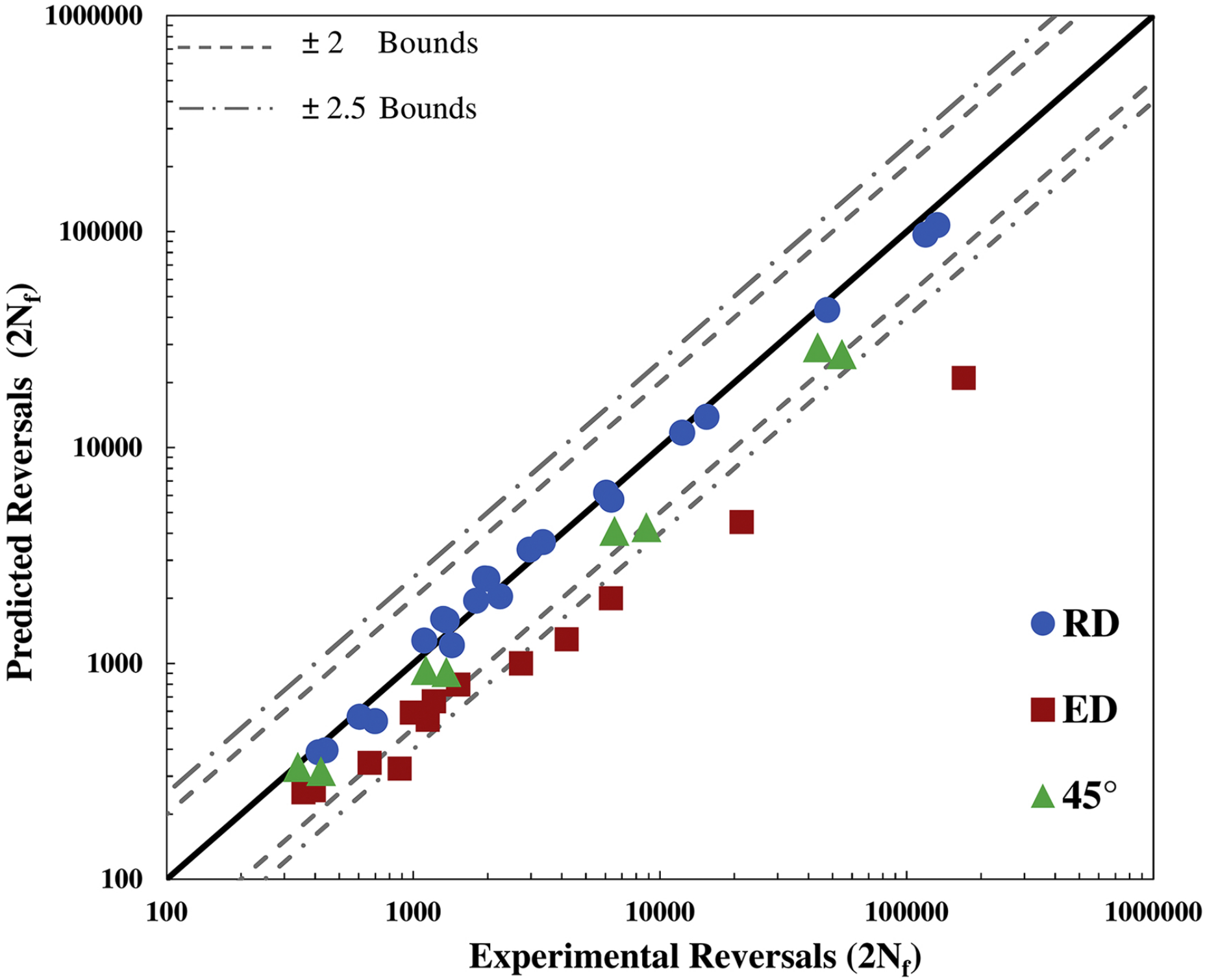
± 2 Bounds
± 2.5 Bounds
RD
ED
45°
Predicted Reversals (2Nf)
Experimental Reversals (2Nf)
100
1000
10000
100000
1000000

Figure 21

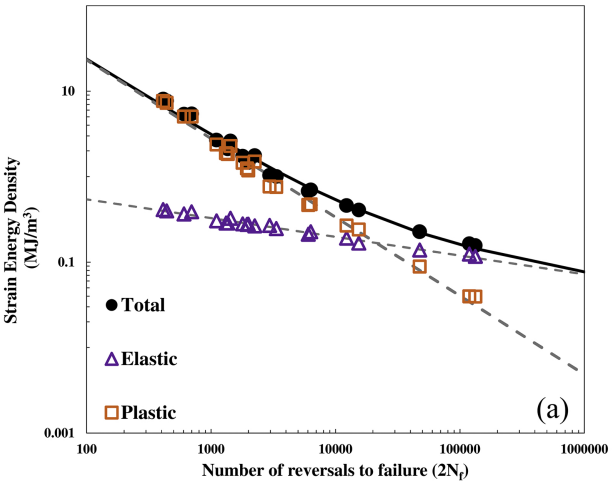
Strain Energy Density (MJ/m³)
10
0.1
0.001
Total
Elastic
Plastic
(a)
100
1000
10000
100000
1000000
Number of reversals to failure (2N_f)

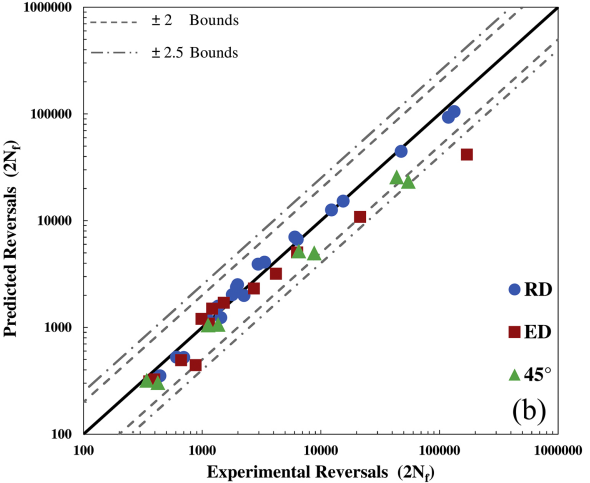
± 2 Bounds
± 2.5 Bounds
Predicted Reversals (2N_f)
1000000
100000
10000
1000
100
RD
ED
45°
(b)
100
1000
10000
100000
1000000
Experimental Reversals (2N_f)

Figure 22

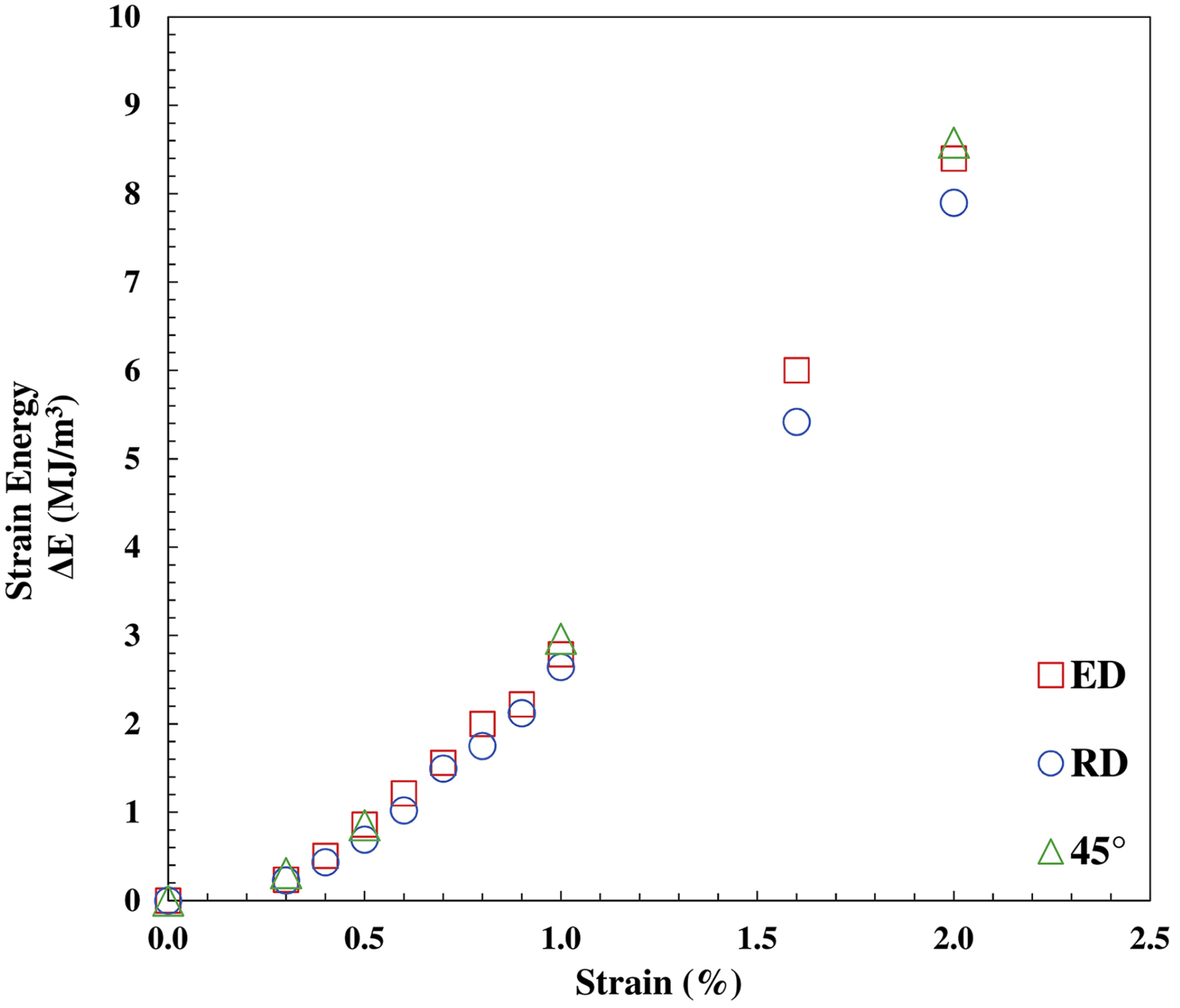
Strain Energy
ΔE (MJ/m³)
10
9
8
7
6
5
4
3
2
1
0
0.0
0.5
1.0
1.5
2.0
2.5
Strain (%)
ED
RD
45°

Figure 23